Figure removed due to copyright restriction

Dielectric breakdown of epoxy and its use as insulation for a high-voltage anode cable connector

By

Aaron Doherty

Academic Supervisor:

Associate Professor Egon Perilli

Industry Supervisor:

Nicco Moncelli, Micro-X

Thesis
Submitted to Flinders University
for the degree of

Master of Engineering (Biomedical)

College of Science and Engineering

17th October 2022

Declaration:

I certify that this thesis:

1. does not incorporate without acknowledgment any material previously submitted for a degree or diploma in any university
2. and the research within will not be submitted for any other future degree or diploma without the permission of Flinders University; and
3. to the best of my knowledge and belief, does not contain any material previously published or written by another person except where due reference is made in the text.

Signature of student..

Print name of student: Aaron Doherty

Date: 17 / 10 / 2022

I certify that I have read this thesis. In my opinion it is/is not (please circle) fully adequate, in scope and in quality, as a thesis for the degree of Bachelor of Engineering (Biomedical) (Honours) / Master of Engineering (Biomedical). Furthermore, I confirm that I have provided feedback on this thesis and the student has implemented it minimally/partially/fully (please circle).

Signature of Principal Supervisor..

Print name of Principal Supervisor: A/Prof Egon Perilli

Date: 17 / 10 / 2022

Acknowledgements:

I would like to thank my academic supervisor Associate Professor Egon Perilli for his assistance throughout the year, for holding me to a high standard and ensuring my work is of high quality, and especially for finding the time for me to use the large volume micro-CT system at Flinders University's Tonsley campus. This thanks extends to Flinders Microscopy and Microanalysis for providing access to the large-volume micro-CT system.

I would also like to thank my industry supervisor Nicco Moncelli, who played no small part in organising the equipment and space I needed to complete my experiments. Also from Micro-X, and in no particular order, I would like to thank Jon Bates, Kym Alexopoulos and Andrew Kuskoff for their aid in understanding the potting process. Additionally, Dr Dylan Thorpe for sharing his patience and expertise in mechanical design. Finally, Susanne Sahlos, Gandalf Du Preez, and Dr Steve Trewartha for their assistance in experiment design and execution.

Executive summary:

Epoxy is an organic polymer that can act as an insulator material for high-voltage applications. By adding non-conductive filler materials, the dielectric properties of the epoxy can be modified. However, published literature is indecisive as to the effect of adding aluminium oxide nano-scale fillers to epoxy will have on the resulting nanocomposite's dielectric properties, especially under direct current (DC) conditions. Most implementations of epoxy as an insulator material are in power systems and involve alternating current (AC) conditions at commercial power frequencies, however medical X-rays are generated using high DC voltages. Thus, it is critical to understand the dielectric properties of epoxy under these conditions.

Samples of bisphenol-A based epoxy with low concentrations of aluminium oxide nanofillers were subjected to ramp voltages up to 120 kilovolts (kV), and the voltage required for the samples to fail recorded. Samples that survived this initial ramp voltage were then subjected to repeated step pulses at 120kV until failure. It was found that neat epoxy (no filler) had the greatest dielectric strength, with nanocomposites with 0.5% nanofiller performing the worst. Higher concentrations of nanofiller (1 and 2%) did not differ from the neat epoxy in a statistically significant way. Sample size was a limiting factor, with only four samples at each concentration produced.

Additionally, a high-voltage anode cable connector was designed and successfully potted using Micro-X's potting techniques. The cable assembly was able to withstand voltages up to 132kV and pass the dielectric strength test as described in the IEC 60601 *Medical Electrical Equipment* standard and survive for over a year and a half of accelerated lifespan testing as of the time of writing. An X-ray image of a watch was produced using a Micro-X X-ray tube powered using this potted cable assembly.

Table of Contents:

List of Figures:

Introduction:

X-rays and their generation:

X-rays are a form of electromagnetic radiation (photons) that are invisible to the human eye. Where visible light has a wavelength of 400-700 nanometres, the wavelength of an X-ray is much shorter, often between 10 to 0.01 nanometres. The energy (*E*) of a photon is given by the following equation:

$$E = \frac{hc}{\lambda}$$

Where *h* is Planck's constant, *c* the speed of light in vacuum, and λ the photon's wavelength (Markowicz, 2001). Thus, a shorter wavelength results in a higher energy photon. X-rays, and all photons with wavelengths shorter than ultraviolet, are considered ionising radiation. These photons possess enough energy that upon impact with an atom, they can induce the release of an electron from its orbit about the atomic nucleus via the photoelectric effect or the Compton scattering process (Leroy and Rancoita, 2011).

X-rays can be generated from a variety of phenomena, both naturally and artificially. Natural causes include lightning, cosmic bodies such as stars, or the natural decay of radioactive isotopes. Photons released from radioactive decay are usually termed gamma rays, however they can possess energies well within the standard range for X-rays (Debertin and Helmer, 1988). Artificial X-rays, first documented by Wilhelm Röntgen in 1895, are produced by the acceleration of electrons to a very high velocity, prior to their impact with a dense metal target such as tungsten. The kinetic energy lost during this impact is mostly converted to heat, with only 1% of the total energy converted to X-rays (Boone, 2000). The production of artificial X-rays, as well as their energy levels, can also be precisely controlled so are more suitable for medical imaging than natural processes.

In addition to cyclotrons and synchrotrons, X-ray tubes are often used to generate X-rays, especially for medical purposes. Like cathode ray tubes and vacuum fluorescent displays, traditional X-ray tubes consist of a heated cathode which supplies the desired quantity of electrons via thermionic emission, which are then attracted to the positively charged anode.

As the tubes are evacuated, electrons can move freely to the anode without interacting with air particles (Arns, 1997). The speed at which electrons can travel is governed by the voltage applied between anode and cathode. An electron-volt (eV) is the amount of kinetic energy gained by an electron when it passes through a potential of one volt from rest. To produce X-rays for medical imaging, electrons must be accelerated at up to 150keV prior to impact (Hasegawa, 1990). Thus in this scenario, a voltage of 150kV would need to be applied across anode and cathode to produce X-rays with energies up to 150keV.

X-ray tubes produced by the company Micro-X, an Adelaide-based company where the research for this project has been carried out, use a cold cathode rather than a heated filament. No thermionic emission of electrons occurs in a Micro-X tube, rather electrons are provided to the tube via field emission – passing a small current over a novel carbon nanotube structure. As a result, the tubes themselves can be manufactured to be lighter and smaller (Fig. 1), more efficient, and with longer lifespans as there is no risk of a cathode filament burning out (Gonzales, 2020).

Figure removed due to copyright restriction

Figure 1 – Size comparison between a traditional heated filament X-ray tube (rear) and a Micro-X CNT X-ray tube (front). The traditional tube weighs about 15kg, whereas the Micro-X tube weighs a mere 2.2 kg (Gonzales, 2020).

Electric fields and stresses:

The presence of electric charge results in a surrounding electric field (E, Fig. 2). Such a field exerts force on other charged particles within the field depending on the polarity and voltage of the charge, imparting a repelling (like charges) or attracting (opposite charges) force upon them (Arora and Mosch, 2022). The exertion of force on material results in stress within that material, and for an electric field this is modelled using the following equations:

$$F = qE$$

$$E = -\nabla\phi$$

Where *E* is the electric field intensity, *q* the charge of a point, and *F* the force at that point. ϕ is the voltage differential at a particular point, with ∇ as defined below:

$$\nabla = a_x \frac{\partial}{\partial x} + a_y \frac{\partial}{\partial y} + a_z \frac{\partial}{\partial z}$$

a_x, a_y, a_z are from the position vector $r = a_x x + a_y y + a_z z$ of the particular point (Naidu, 2013). The SI unit for electric field intensity is Volts per meter.

Figure removed due to copyright restriction

Figure 2 – Visualisation of an electric field about two particles. The lines are equipotential lines, each point on such a line has the same voltage. Image source: https://commons.wikimedia.org/wiki/File:VFPt_charges_plus_minus_thumb.svg#/media/File:VFPt_charges_plus_minus_thumb.svg

Insulating materials and their failure:

As contact with high voltages can be very dangerous, causing severe injury or death, such voltages should be kept insulated from their surroundings. This requires the use of insulation material with a high dielectric strength – the ability to withstand high electric field stress without failure (Holtzhausen and Vosloo, 2014). Solids, liquids, and gasses can all be used as insulating materials. Some common materials used for high-voltage insulation include ceramics, sulphur hexafluoride (SF^6), and resin epoxies (Berger, 2006). However, should the applied voltage be greater than the dielectric strength of a material, breakdown can occur in which atoms within the material are sufficiently ionised to the point they conduct electricity rather than insulate. This process is known as dielectric breakdown.

Often preceding full dielectric breakdown is the phenomenon of partial discharge. At points of divergent electric fields, regions of the insulation material can experience localised breakdown, however this is not severe enough to completely bridge between conductors (Niemeyer, 1995). In gaseous insulators, this process is observed as corona discharge – a glowing plasma around a conductor present at locations where the electric field stress is greater than the dielectric strength of the gas (Chang et al., 1991). In solids, the continued partial breakdown of an insulator can result in spectacular 'trees' being formed within the material; however, this is undesirable as it eventuates in the failure of the insulation.

Figure removed due to copyright restriction

Figure 3 – Example of electric treeing propagating through a polyethylene sample. Note the pointed electrode indicated in red where the tree initiates (Azizian Fard et al., 2019).

In solid insulators, diverging electric fields occur where voids or impurities are present in the material, as the dielectric constants of the insulator and impurities will likely vary. Thus, this is where partial breakdowns are most likely to initiate. Additionally, sharp points such as the pointed electrode in Fig. 3 will concentrate the voltage gradient and enhance the electric field divergence at these points (Osmokrovic et al., 2005). As two conductors separated by an insulator form a capacitor, the high-voltage system can be modelled as a variety of different capacitances (Fig. 4), highlighting the effect of voids or impurities within the solid dielectric.

Figure removed due to copyright restriction

Figure 4 – Model capacitances of a solid dielectric with a void (Pan et al., 2019).

The capacitance of the void is much lower than the other capacitances of the surroundings, and as capacitors in series share a constant charge, there is a much higher voltage gradient across the smaller void capacitance (Lemke, 2012). This is demonstrated in the following equation:

$$V = \frac{Q}{C}$$

Where V is the voltage, Q the charge and C the capacitance. Thus, with a tiny capacitance, the voltage drop across the void is significant, and can lead to the initiation of partial discharges at the boundary between void and insulator (Kind and Kärner, 1985). Just like a standard capacitor, insulators act differently under alternate current (AC) conditions than when under direct current (DC) conditions. Due to this, the breakdown voltage of a material under DC conditions is usually greater than the breakdown voltage of the same material under AC conditions (Seong et al., 2012).

Non-conductive filler particles:

The breakdown voltage of insulators can be further improved by the addition of non-conductive filler particles at the micro- or nano-scales (Babu et al., 2019). Epoxies with such added fillers are referred to as microcomposites or nanocomposites. Micro-X currently use a two-part, bisphenol-A resin epoxy with calcium carbonate / barium sulfate ($CaCO_3$/$BaSO_4$) microparticle filler for encapsulation of a custom high-voltage generator. Bisphenol-A is the preferred base, as it has excellent mechanical properties and is a milder exotherm (Wetherill et al., 2007). Other inorganic fillers commonly used for high-voltage insulation applications include silicon dioxide (SiO_2), aluminium oxide (Al_2O_3, or alumina), titanium dioxide (TiO_2) and zinc oxide (ZnO), and these fillers can also improve mechanical properties of resin epoxy (Kitichatpayak et al., 2022). Additionally, de-gassing resin epoxies under vacuum reduces the size and likelihood of air bubbles (voids) persisting in the cured product, lowering risk of breakdowns (Afendi et al., 2005).

The "Micro-X Rover" is a mobile X-ray imaging device that utilises Micro-X's novel carbon nanotube X-ray technology. It requires 110kV of potential across the tube anode and cathode to produce X-rays, which is directed to the tube using a third-party HV cable produced only for Micro-X by Varex Imaging (Salt Lake City, Utah, USA). Notably, X-ray tubes designed by Micro-X require DC current for operation. As part of a cost reduction process, as well as for future research applications (such as more advanced insulating solutions), Micro-X are interested in the feasibility of producing and insulating the connector interface of a similar cable using in-house potting techniques. The currently used anode cable, manufactured by the company Varex, terminates in a right-angled 'pancake' style connector (Fig. 5) with a centre conductor, epoxy dielectric, and an outer casing that acts as ground. It is important that the epoxy on the interfacing surface is as flat as possible to reduce field stress.

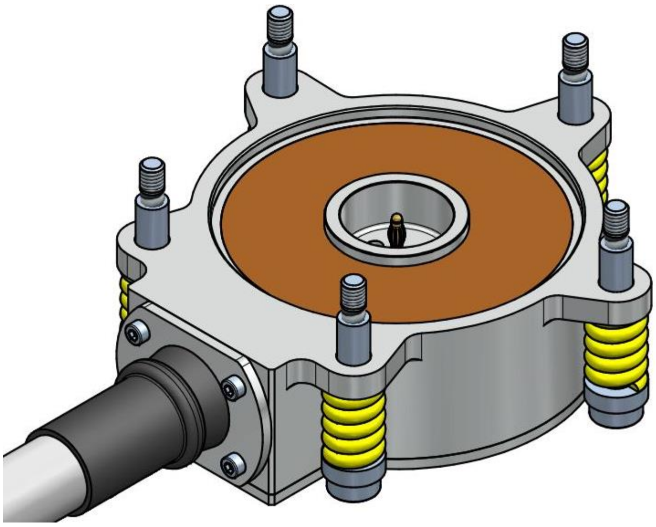

Figure 5 – Render of the Varex pancake connector. The top surface is the interfacing surface.

Micro-X have refined a vacuum-casting technique, in which epoxy is drawn into a vessel through a pressure differential between vacuum chambers. This allows for the entire mixing and casting process to be undertaken without exposure to air, preventing voids or bubbles. Resin epoxy is injected into the bottom of the vessel, flowing upwards and out of a release hole at the top of the vessel. This helps ensure that epoxy has filled the entire volume of the vessel. Additionally, an actively cooled, removable 'shut-off' plate is used to control the flatness of the epoxy interface surface by reducing thermal expansion during exotherm where temperatures have been recorded exceeding 70°C for Micro-X products (Fig. 6).

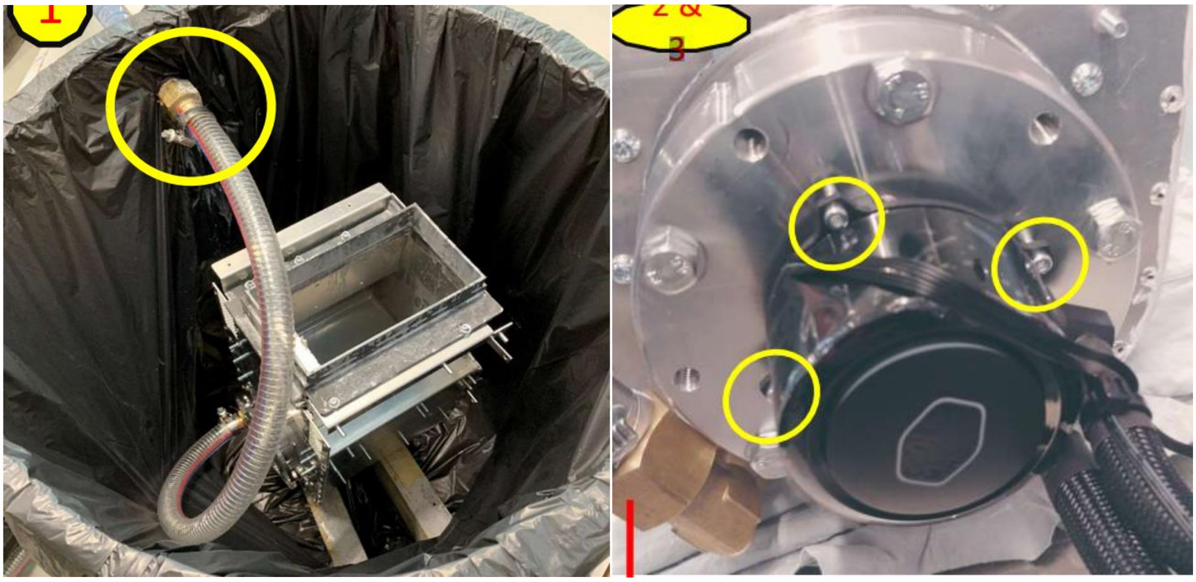

Figure 6 – A high-voltage generator about to be potted using the bottom-injected vacuum cast technique (left) and a shut-off plate with cooling solution installed (right).

Literature review:

Nanofillers and their effects on the dielectric strength of epoxy insulators:

Initial research outlining the potential usage of nanofillers to improve the dielectric strength of insulation material was first proposed nearly 30 years ago (Lewis, 1994). Since then, there has been growing research into the electrical properties of micro- and nanocomposites, yet a consensus has not yet been reached, on whether or not the addition of these filler particles has the desired effect of increasing the breakdown voltage of resin epoxy, especially under DC conditions (Paramane and Kumar, 2016).

Imai et al. conducted experiments on the breakdown voltages of bisphenol-A resin epoxy with and without nanofiller and concluded that there was little difference. **SiO_2** and **Ti_2** nanoparticles were used as filler material at 5 weight percentage (written as “wt%” in the remainder of the thesis), with tests performed under AC conditions from 50 to 1kHz (Imai et al., 2006). Mohanty et.al determined that the addition of 2% by weight **Al_2O_3** nanoparticles to an epoxy sample increased the AC breakdown voltage by 91%, and 5% Al_2O_3 nanoparticles increased the breakdown voltage by 155% when compared to neat epoxy (Mohanty and Srivastava, 2013). The breakdown voltage at 5% was approximately 28kV/mm, and these tests were conducted as per the standard ASTM D3756-97(2010) i.e., at mains power frequencies (50-60Hz).

The results by Mohanty are contrasted by research conducted by Preetha et al., who showed that low levels (0.1 wt% and 1 wt%) of **Al_2O_3** nanofiller in bisphenol-A reduces the AC breakdown strength. However, 5 wt% of nanofiller improved the breakdown strength similar to Mohanty et al., and at levels greater than 10 wt%, the breakdown strength decreased once again (Preetha and Thomas, 2011). Yet, insignificant differences in the dielectric strength of nanocomposites have also been reported at nanofiller concentrations of 2.5 and 5 wt% when compared to neat (Iyer et al., 2011). Wang et al. undertook experiments by applying a pulse voltage to resin samples with 0, 1, 2 and 5 wt% Al_2O_3 nanofiller, and once again yielded a different result. In their experiments, 1 wt% Al_2O_3 nanofiller provided a superior breakdown voltage than neat epoxy and higher concentration nanocomposites (Wang et al., 2019b). The breakdown voltage at 1 wt% was about 6kV/mm, and at 5 wt% it was 5.5kV/mm, far less than that reported (28kV/mm) by Mohanty et al.

Research into the effect of **SiO_2** micro and nanoparticles on the breakdown voltage of low-density polyethylene (LDPE) conducted by Yin et al., provided further evidence that under DC conditions, the nanocomposite had greater breakdown strength than neat LDPE. However, this trend reversed at higher concentrations of SiO_2, with 0.5% and 1% by weight of SiO_2 providing the most benefit, whereas at 5% this effect was diminished (Yin et al., 2007). Once again there is contrasting literature, with research showing that SiO_2 nanofillers in the range of 6-8 wt% yielding better breakdown strength than lower or higher concentrations (Ramu and Nagamani, 2014). This paper also looked at Al_2O_3 and determined SiO_2 was the superior nanofiller under their DC voltage testing conditions.

Further doubt on the ideal ratio of nanofiller for DC applications is cast by Wang et al., who demonstrated **Al_2O_3** nanofillers in a bisphenol-A base had the highest breakdown voltage at a 1 wt% concentration (Wang et al., 2019a). The breakdown voltage increased from 0 to 1%, then decreased from 1 to 5%.

Contrasting with Ramu's conclusion, that 6-8 wt% of **SiO_2** nanofiller was ideal under DC conclusions, Kochetov et al. had best results when a mere 0.5 wt% of SiO_2 nanofiller was used. Both researchers used a degassed bisphenol-A resin epoxy as base, and applied DC voltage (Kochetov et al., 2014). Kochatev's team previously had similar results with MgO and Al_2O_3 nanofillers, with 0.5 wt% found once again to provide the highest strength (+61% vs neat) for both additives (Andritsch et al., 2010).

The type of nanofiller used to dope resin epoxy also influences its dielectric properties. The previously mentioned study by Ramu et al. found that SiO_2 was superior to Al_2O_3 for this purpose, and a previous study by Singha et.al found that dielectric strengths of TiO_2 nanocomposites were lower than Al_2O_3 nanocomposites at the same concentrations, under

AC conditions (Singha and Thomas, 2008). A review on the three most common additives in published research (Al_2O_3, TiO_2, and SiO_2), found that for those studies that exhibited an increase in breakdown strength, Al_2O_3 afforded a higher breakdown voltage than the other nanoparticles (Adnan et al., 2019).

Nanocomposites versus microcomposites:

Nanocomposites have shown to be more effective at increasing the breakdown strength than microcomposites, with 5% (by weight) Al_2O_3 nanoparticles recording greater partial discharge resistance than 60% Al_2O_3 microparticles (Li et al., 2010). Similar results were obtained by Nelson et al., who showed that the use of TiO_2 nanoparticles in bisphenol-A epoxy, yielded an increase in the breakdown voltage of the sample, whereas the use of microparticles demonstrated a decrease (Nelson et al., 2003). Additionally, the use of Al_2O_3microfiller alone was shown to reduce breakdown strength beyond concentrations of 40 wt%, yet when 60 wt% of Al_2O_3microfiller was combined with 1% nanofiller breakdown strength more than doubled (Park et al., 2015).

Cheng et al. provides further supporting evidence, showing that LDPE doped with ZnO nanofiller had superior breakdown strength compared to ZnO microfiller (+11% vs -1.3%) at the same concentration. In fact, the use of microfiller resulted in reduced breakdown strength to the point that neat LDPE was superior (Cheng et al., 2020). MgO in LDPE showed similar results under DC conditions, with the nanocomposite once again demonstrating superior breakdown strength compared to the microcomposite, to the point where the researchers recommend using the nanocomposite (Okuzumi et al., 2008).

Under positive DC, the breakdown voltage of epoxy nanocomposites is greater than the breakdown voltage of the same sample subjected to negative DC (Sarathi et al., 2007). Similar results have been obtained in bisphenol A using Al_2O_3fillers (Fujita et al., 1996, Okabe et al., 2015). However, the breakdown voltage of air, which of course may be present in resin epoxy mixtures, is greatest under negative DC voltages (Kara et al., 2010). The occurrence of this process over sub-mm air gaps is further supported by (Hogg et al., 2013).

Epoxy used by Micro-X:

Micro-X have developed their own potting method to insulate their custom high-voltage generator, known internally as the 'Cooper'. The insulating material is a unique, two-part (base and hardener) bisphenol-A resin epoxy with $CaCO_3/BaSO_4$ microparticle filler provided by domestic supplier Megapoxy. This resin epoxy is designed for a low exotherm reaction to prevent shrinkage (pull-off) during curing, a process by which the epoxy separates from its surrounds, leaving voids (Kohl and Singer, 1999).

Potting process:

Micro-X have refined the potting of their generator by degassing both the base and hardener for at least 24 hours, not only removing air present in the epoxy, but also lowering the pressure of any air that remains. As per Paschen's law, the following equation describes the effect of reducing pressure on the breakdown voltage of any remaining gasses:

$$V_b = \frac{Bpd}{\ln\left(\frac{Apd}{ln\left(1+\frac{1}{\gamma}\right)}\right)}$$

V_b represent the breakdown voltage of a gas, pressure is represented by p and distance by d. A, B and γ constants (Husain and Nema, 1982). Thus, as the pressure of a gas decreases, so does the breakdown voltage, until a critical point is reached where the breakdown voltage increases rapidly with minor pressure decreases. A Paschen curve (Fig. 7) is the best method to visualise how these parameters interact:

Figure removed due to copyright restriction

Figure 7 – Paschen curve of various gasses (Burm, 2007).

The base and hardener are then mixed under vacuum for a few minutes inside a bucket with a hole in the bottom, connected to a short piece of hose. The other end of this hose is connected to the base of a Cooper generator, also under vacuum. Once the high-voltage generator is released from vacuum, the epoxy flows through the hose due to the pressure difference and begins to encapsulate the generator from the bottom-up; this ensures there are no voids on the underside of any electrical components, as may occur if the epoxy was simply poured in from the top.

It is crucial that the epoxy does not pull-off from the high-voltage connector interface, as otherwise the electric field stresses will amplify in these non-uniform regions (Haddad et al., 2004). To combat this, a cooling plate is attached to the connector interface, which is actively cooled using a simple radiator commonly used to cool consumer computer chips. Thus, the epoxy at this location is kept at a reduced temperature, reducing its thermal expansion whilst setting and decreasing the likelihood of pull-off occurring upon cooling. Such shrinkage processes are well documented in literature (Chekanov et al., 1995, Khoun and Hubert, 2010, Zarrelli et al., 2002).

Figure removed due to copyright restriction

Figure 8 – A visualisation of electric field stresses about a needle tip. Despite being firmly located in the blue lower-stress region, the small void on the right experiences quite high stress (Balachandran et al., 2017).

As voids present within epoxy insulators are of great concern (Fig. 8), methods for detecting them prior to the application of high voltage are necessary. Recent work by Rojek et al. showed that computed tomography (CT) was appropriate for the detection of voids in a bisphenol-A epoxy resin. However, only neat epoxy was investigated Rojek et al. (2020). A similar study, also using bisphenol-A but with glass spheres as filler, found that void volume could be calculated quite easy; the epoxy did not attenuate the X-rays (Awaja et al., 2009). Micro-CT at a resolution of 8µm has also been used to discern voids around regions of interest, however this was with an epoxy thickness of only 4mm (Scott et al., 2014). There is also much research on the use of CT to determine voids in carbon fibre or fabric epoxy composites (Léonard et al., 2012, Sisodia et al., 2016). However, there is little research into the CT imaging of resin epoxy with Al_2O_3, TiO_2, and SiO_2 fillers. Hughes et al. did use X-ray tomography to investigate the dispersion of TiO_2 filler in epoxy rather than search for voids in the sample. There is no mention of filler size in the paper (Hughes et al., 2012).

Gap analysis:

Much is known about mechanical and thermal characteristics of bisphenol-A based resin epoxies, both with and without filler particles.

Research gap 1: No real consensus has been reached in the community regarding the breakdown voltage of aluminium or titanium oxide nanocomposites, with many published results contradicting each other (Adnan et al., 2019). Additionally, with identical percentages of nanofiller, aluminium oxide seems to have varying effects on the breakdown voltage of resin epoxy, with different studies achieving opposite results (Kochetov et al., 2014, Ramu and Nagamani, 2014, Wang et al., 2019a).

Research gap 2: The DC breakdown voltage for TiO_2 nanocomposites is lacking data for concentrations under 5 wt% (Ghouse et al., 2013). Manufacturers often provide only an AC breakdown voltage rating for epoxy/insulator products, however, there is no reliable way to convert these AC breakdown values to an appropriate DC breakdown voltage (Wu et al., 2017). The same is true for the DC breakdown voltage of Al_2O_3 nanocomposites, with only Andritsch et al. (2010) publishing results for 0.5 wt%. Further research into the DC breakdown strength of nanocomposites is required for improved safety and effectiveness of insulating materials used in the high-voltage connector of the Micro-X Rover.

The Micro-X potting process has not yet been tested for small volumes or cable connector geometries. Insulation of a system against high-voltage requires good design choices and the avoidance of voids or other impurities in the insulator material to prevent partial breakdowns (Shibuya et al., 1977). Nor has there been much CT scanning of resin composites using metal oxide fillers, with only one study looking at TiO_2 microfiller dispersal rather than searching for voids (Hughes et al., 2012).

Aims:

The primary objective of this thesis is to measure the DC breakdown voltage and quantity of partial discharge events preceding breakdown of epoxy resin containing 0% (neat), 0.5%, 1% and 2% Al_2O_3 by weight nanocomposites. This is due to the conflicting published literature regarding the effect of adding Al_2O_3 nanoparticles on the dielectric properties of bisphenol-A resin, as well as to the lack of literature on DC breakdown for nanocomposites with nanofiller concentrations at 2wt% or under.

The secondary objective is to design and encapsulate a high-voltage anode cable connector for use with the Micro-X Rover high-voltage generator and X-ray tube, using the Micro-X potting processes. To evaluate the performance of the potted connector, it will be tested against the requirements as set out by the IEC60601 *Medical Electrical Equipment* standard, as well as subjected to a year of accelerated life testing (ALT), to replicate heavy daily use. Finally, the anode cable will be connected to an X-ray tube and an X-ray image taken.

Methodology (Aim 1) – Dielectric strength testing of epoxy with different alumina nanofiller concentrations:

The aims of this experiment were as follows:

- To determine the DC breakdown voltage of resin epoxy samples with Al_2O_3 nanofiller at concentrations of 0% (neat), 0.5%, 1% and 2% by weight.
- To record the quantity and measure the peak magnitude (in volts) of any partial discharges that may occur in these samples, over the duration of the tests.

Preparation of epoxy and electrodes:

Bisphenol-A based resin epoxy (CAS number: 25068-38-6) was mixed with Al_2O_3 nanoparticles of size less than 50nm (AEROXIDE® *Alu C* – CAS number: 1344-28-1) by Megapoxy (Thornleigh, NSW) in concentrations of 0% (neat), 0.5%, 1% and 2% $Al_2O_3$by weight. This nanocomposite will be referred to as 'Part A' and forms the bulk of the epoxy. An epichlorohydrin-based hardener 'Part B' (CAS number: 68410-23-1) was also provided by Megapoxy. Due to time and material sourcing constraints, only nanocomposites using Al_2O_3 were obtained.

Brass electrodes as per ASTM D149-20 *Standard Test Method for Dielectric Breakdown Voltage and Dielectric Strength of Solid Electrical Insulating Materials at Commercial Power Frequencies* were produced. This standard was used as no standard for testing under DC conditions exists. These electrodes are opposing cylinders 25mm in diameter, 25mm thick, and edges rounded to a 3.2mm radius, and are the suggested electrode chape for epoxy according to the standard. Tests conducted by Monzel et al. (2015), Martin et al. (2007) and Amin et al. (2016) utilised this type of electrode. The surfaces were polished, and one end of each electrode had 10mm of M5 thread for mounting to the testing setup and electrode moulds. The two electrode moulds allow for the brass electrodes to be held 3mm apart; this was the sample thickness used in experiments by Preetha and Thomas (2011).

A Spellman "ST" high-voltage generator capable of producing up to 120kV with a ramp rate of 90kV/second was obtained and interfaced to an enclosed metal pot filled with an insulating mineral oil (Shell *Diala S4 ZX-1*). Use of insulating oil is recommended in ASTM D-149-20 to prevent surface flashover during testing (Iyer et al., 2011). The output of the Spellman was connected to a curved aluminium rod with M5 tapped threads to allow interfacing to the brass electrodes, as well as hold the samples away from the Spellman cable receptable and the outside of the metal pot to avoid arcing (Fig. 10). At the other end of the epoxy sample, an earth wire was attached to complete the circuit. This earth wire passes through a current transformer which itself is connected to an input channel of a Picoscope (Model *3406D*, 1GHz sample rate). The Picoscope was configured to begin logging upon any detected current and interpret the next 200ns of discharge activity as a single event. The entire oil pot setup was within an interlock box, connected directly to the power supply of the Spellman to ensure high voltage could not be enabled if the box was open.

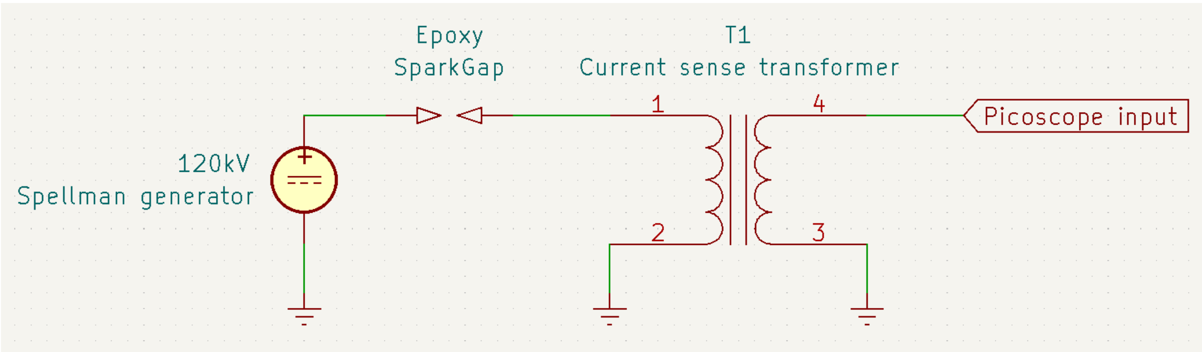

Figure 9 – Electrical diagram of the experimental setup.

Figure 10 – Underside of metal pot lid used in the experiments (left) and the oil pot within an opened interlock box for safety (right). The gentle curve of the aluminium rod is for electric field control.

Resin preparation and potting

For each of the concentrations (neat, 0.5%, 1%, 2%), four samples were prepared.

The resin epoxy itself was prepared as per the Micro-X method outlined in STS314 "*Potting material preparation".* This process involves calculating the required mass of parts A and B, then pouring the appropriate mass of each into separate buckets. For these tests, 500ml of epoxy was to be prepared each time the two moulds were to be filled, as any smaller quantities would be too difficult to handle properly. This results in 645.8g of part A and 129.2g part B per batch for a 5:1 weight ratio.

Each bucket was then degassed at 2500 Pa (~0.025 standard atmospheres) for 48 hours in the Micro-X vacuum chambers. Temperature within these chambers was held at 26°C throughout. When degassing was complete, the buckets were removed and part A poured into the bucket containing part B, and the components were gently mixed by hand using a plastic rod for 10 minutes. This differs from the Micro-X process where the components are both combined and mixed under vacuum, however with the small volumes used in preparing the epoxy samples this was not possible. The Micro-X process involves the use of transfer pipes and metallic mixing blades, which were too large to be used here. After mixing, the resin epoxy was degassed for 30 minutes in a vacuum chamber.

Whilst the resin epoxy was degassing, the electrode moulds were prepared. Both moulds were thoroughly cleaned with isopropyl alcohol before two coats of mould release were applied onto the surfaces that would contact resin epoxy. O-rings were fitted once the mould release had dried, and an electrode was placed in each half. A nut was used on the exposed electrode thread to hold the electrode at the correct spacing, then the two halves of the mould fastened together. The degassed resin epoxy was injected into the mould using a 10ml syringe, the excess epoxy was discarded. Again, this differs from the Micro-X potting process, where resin is injected whilst under vacuum. The injected moulds were then returned to the vacuum chamber to cure for at least 48 hours. This process was repeated 8 times, yielding 16 epoxy/electrode samples consisting of 4 of each concentration - 0%, 0.5%, 1% and 2%.

“Megapoxy E Slow”: an additional two samples of “Megapoxy E Slow” were also potted. Of note, these samples were potted using excess epoxy from the potting of a Cooper generator, and thus were mixed under vacuum using a mechanical stirrer, rather than by hand.

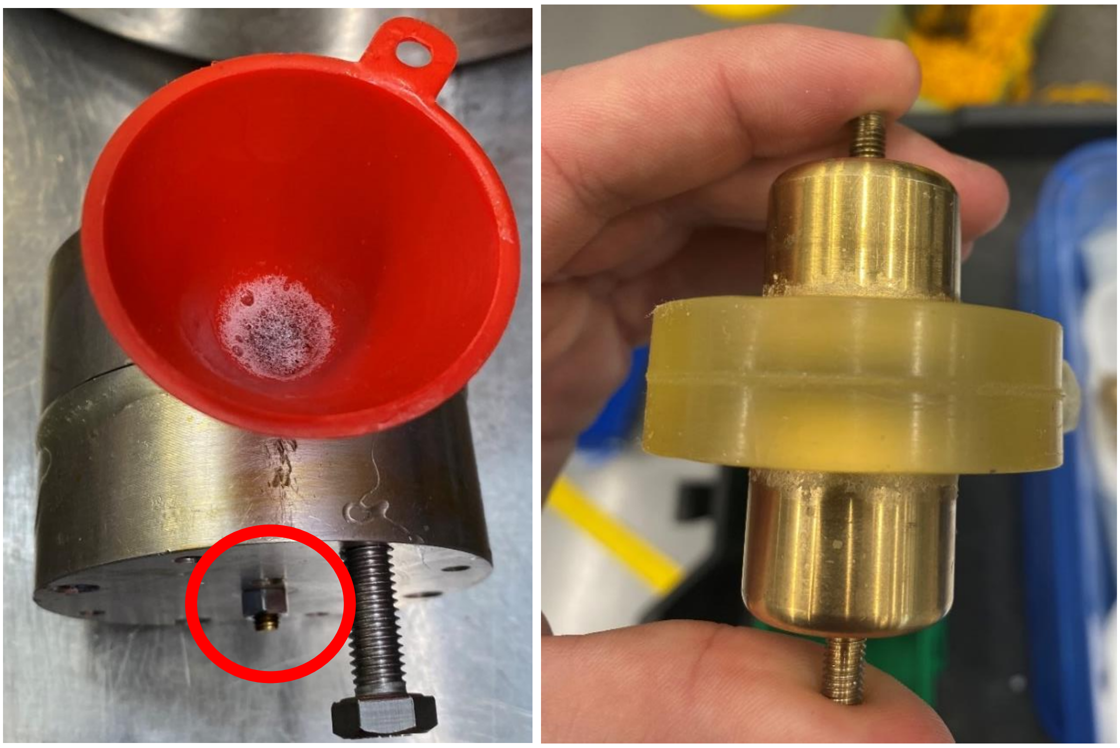

Figure 11 – A filled electrode mould (left) and a cured sample of neat epoxy (right). Note the small nut (red circle) holding the brass electrode thread in place (left image).

Withstand test – Slow ramp to 120kV at 1kV per second, then a 60 second hold at 120kV:

Outcome measure: Voltage read out (using Spellman control software, explained in paragraph “Spellman pulse logs” below), if an arc was detected (indication of failure). Each sample (four samples at each of four different nanofiller concentrations) was fastened to the aluminium rod connected to the Spellman cable receptable on one end, and the earth wire fastened to the other end of the sample. Then, using custom Spellman control software developed by Micro-X and Resonate Systems (Adelaide, SA) the Spellman was current limited to 1mA, and a withstand test was performed on the sample. This test applies a ramp pulse of 1kV/second to the sample over 120 seconds, then holds at 120kV for 60 seconds before removing the voltage. 120kV is the maximum voltage output of the Spellman generator; if a generator capable of producing higher voltage was available, it would have been used instead. The Picoscope was set to trigger on any measurement greater than twice the background noise as per Wooi et al. (2015), as well as save the preceding 200 voltage samples and following 10000 voltage samples.

Accelerated life testing (ALT - repeated step pulses at 120kV)

Outcome measure: number of pulses (using Spellman control software, explained in paragraph “Spellman pulse logs” below) before an arc was detected (indication of failure). Samples that survived the withstand test were subjected to accelerated life testing, in which step pulses of 120kV DC were applied to a sample for 2 seconds before a 4 second pause to discharge fully. Step pulses (at a ramp rate of 90kV/ms) were applied, as this in combination with the 2 second hold most closely represents the application of DC voltages. This process was repeated for 21,900 cycles (1 year of heavy use at 60 shots a day) or until the Spellman generator detected an arc. Whilst the Spellman is current limited to 1mA, any arc will quickly force the supplied voltage down. The Spellman disables high voltage when an arc is detected whilst the software records pulse logs automatically. Again, the Picoscope was configured to log any partial discharge events during testing.

Spellman pulse logs (Spellman control software):

After a failed test, the Spellman pulse logs were analysed to determine at which voltage setpoint an arc was detected. The pulse logs provide details such as time, kV setpoint, arc detection, overcurrent detection, system faults and 20 other factors into a file exportable into Microsoft Excel. By examining the pulse log for a failed test, the row in which the ‘arc-detected’ column transitions from 0 to 1 is considered as when the breakdown occurred, with the ‘kv-setpoint(kV)’ value of this row considered to be the **breakdown voltage** of that sample. Should the sample fail during accelerated life testing, the **number of cycles** it was subjected to before failure is recorded instead. As the withstand test occurs prior to ALT, and both tests were conducted at the same voltage, completing a withstand test successfully counted as a pulse for ALT purposes.

Statistical Analysis:

For each of the concentrations (neat, 0.5%, 1%, 2%), four samples were prepared, creating four groups containing four samples each. Each sample was subjected to the withstand test and, if it had not yet experienced breakdown (no arcs detected by the Spellman software), then also to accelerated life testing. The four groups (neat, 0.5 wt%, 1 wt%, 2 wt%) were compared for differences in voltage read out and number of pulses by using a Kruskal Wallis non-parametric statistical test. If statistically significant, comparisons were then made between the neat group and each of the groups containing nanofillers through the use of a Mann Whitney non-parametric test. Statistical significance was defined as $p<0.05$, and analysis was performed using MATLAB 2019b.

	A	B	C	D	E	F	G	H	I
1	absolute-time	pulse-time (ms)	kv-setpoint (kV)	ma-limit (mA)	power-on	hv-on	arc-detected	interlock-closed	over-current-trip
2	15/09/2022 03:03:43.096 PM	40	0	1	1	1	0	1	0
3	15/09/2022 03:03:43.136 PM	80	0	1	1	1	0	1	0
4	15/09/2022 03:03:43.176 PM	111	0	1	1	1	0	1	0
5	15/09/2022 03:03:43.216 PM	152	0	1	1	1	0	1	0
6	15/09/2022 03:03:43.256 PM	194	0	1	1	1	0	1	0
7	15/09/2022 03:03:43.296 PM	235	0	1	1	1	0	1	0
8	15/09/2022 03:03:43.347 PM	286	0	1	1	1	0	1	0
9	15/09/2022 03:03:43.397 PM	336	0	1	1	1	0	1	0
10	15/09/2022 03:03:43.437 PM	377	0	1	1	1	0	1	0
11	15/09/2022 03:03:43.477 PM	417	0	1	1	1	0	1	0
12	15/09/2022 03:03:43.517 PM	459	0	1	1	1	0	1	0
13	15/09/2022 03:03:43.556 PM	499	0	1	1	1	0	1	0
14	15/09/2022 03:03:43.597 PM	539	0	1	1	1	0	1	0
15	15/09/2022 03:03:43.636 PM	579	0	1	1	1	0	1	0
16	15/09/2022 03:03:43.677 PM	620	0	1	1	1	0	1	0
17	15/09/2022 03:03:43.718 PM	661	0	1	1	1	0	1	0
18	15/09/2022 03:03:43.757 PM	692	0	1	1	1	0	1	0
19	15/09/2022 03:03:43.796 PM	732	0	1	1	1	0	1	0
20	15/09/2022 03:03:43.837 PM	774	0	1	1	1	0	1	0
21	15/09/2022 03:03:43.876 PM	815	0	1	1	1	0	1	0
22	15/09/2022 03:03:43.916 PM	855	0	1	1	1	0	1	0
23	15/09/2022 03:03:43.957 PM	896	0	1	1	1	0	1	0
24	15/09/2022 03:03:44.007 PM	946	0	1	1	1	0	1	0
25	15/09/2022 03:03:44.046 PM	989	0	1	1	1	0	1	0
26	15/09/2022 03:03:44.091 PM	1029	0.028235531	1	1	1	0	1	0
27	15/09/2022 03:03:44.128 PM	1069	0.068572005	1	1	1	0	1	0
28	15/09/2022 03:03:44.188 PM	1124	0.124034656	1	1	1	0	1	0
29	15/09/2022 03:03:44.246 PM	1187	0.187564601	1	1	1	0	1	0

Figure 12 – Spellman pulse log data during a ramp pulse; only a few columns are shown.

Methodology (Aim 2) – Design and encapsulation of high-voltage connector:

For the secondary aim of this thesis, a cable connector is to be produced, which is then potted in-house at Micro-X. An understanding of the manufacturing and potting processes must be obtained, including determining the effectiveness of the encapsulation. The high-voltage anode cable must interface to both the Micro-X Rover's X-ray tube and high-voltage generator. A full redesign of the connector interface on both the tubes and generator is not feasible, as these parts are currently in production and have been already validated. Thus, the design of this connector must take heavy inspiration from the Varex connector mentioned in the introduction (Fig. 4). Controlling exothermic reaction to prevent pull-off is necessary for a successful pot. As the exotherm temperature and time to peak temperature of curing resin epoxy both increase with an increase in volume (Bero and Plazek, 1991, Becker et al., 2003), due to the small volume an anode cable connector (~200mL), pull-off may not be a concern. For contrast, the Cooper generator requires 10.5L of resin epoxy to fully encapsulate it.

Determining the temperature of the exotherm reaction during epoxy cure:

Arduino code to measure and serially transmit a temperature reading obtained from a thermistor every 30 seconds was developed and tested by the author of this thesis. Over a trial period of 6 hours, the Arduino temperature reading was consistently within 0.3 °C of the thermostat temperature at the Micro-X tube manufacturing facility (23 °C), this was deemed acceptable. A Python script was also developed to read the serially transmitted data and log it in a text file. A proxy connector of similar volume and size to the Varex connector was then 3D printed out of nylon (Eiger's *Onyx* material) and a shut-off plate (PFA coated aluminium) used to pot Cooper generators was obtained. The parts were thoroughly cleaned using IPA, and electrical tape was applied to the underside of the components to present resin epoxy leakage, and more tape applied to the top of the connector to prevent resin epoxy overflow. Excess "Megapoxy E Slow" resin epoxy from a Cooper generator pot occurring simultaneously was then slowly poured into the top of the proxy connector until it was full. The temperature sensor was then quickly attached and taped to the middle of the shut-off plate, then the experiment left to log data over the weekend (approx. 70 hours).

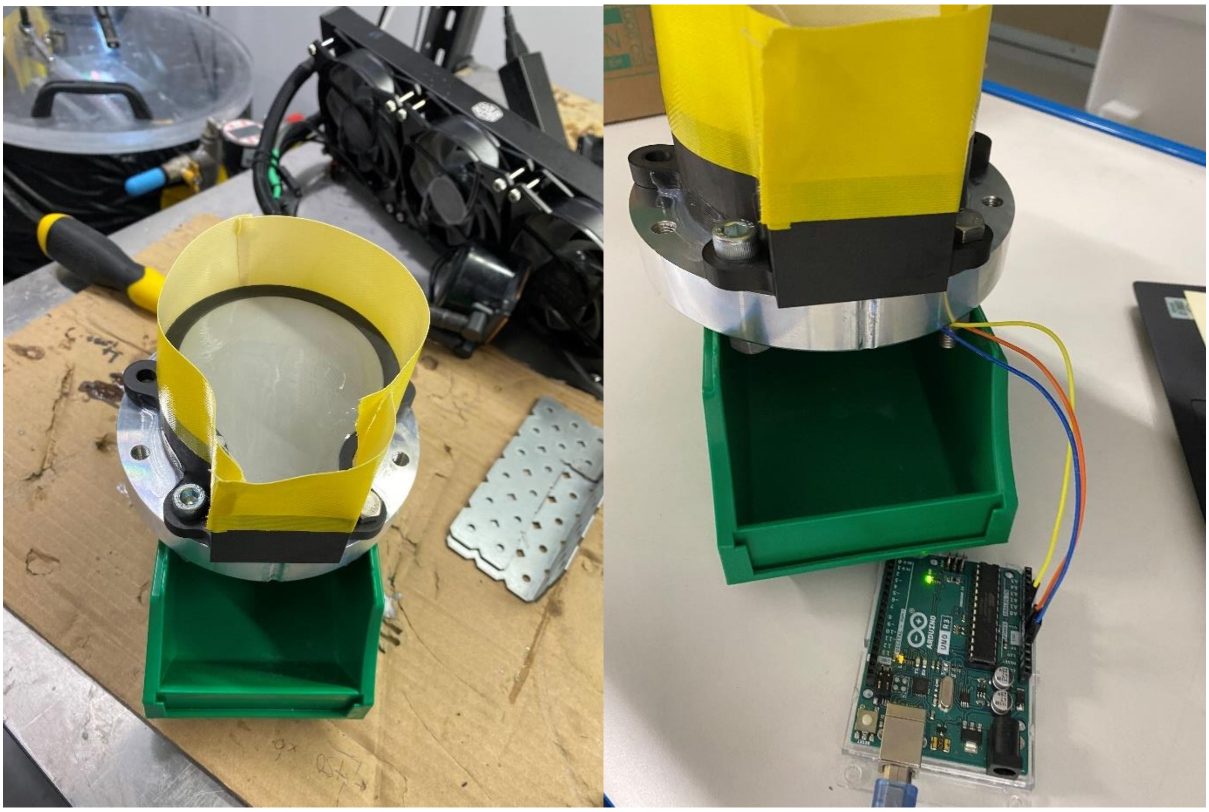

Figure 13 – A view of the potted proxy connector (left) and the Arduino setup (right).

As the anode cable connector requires the termination of a high-voltage cable it is crucial to understand the epoxy flow around this cable, as well as other internal components such as the centre conductor pin. Another proxy connector with the cable and centre pin included was 3D printed, alongside a shut-off plate. Both components were cleaned thoroughly with IPA, mould release was applied to the shut-off plate, and the components interfaced together with a layer of silicon grease to prevent leaks. Again, the proxy connector was taped around the top to prevent resin epoxy overflow. Excess resin from another simultaneous Cooper generator pot was used to fill the proxy connector by slowly pouring resin epoxy from above, then the proxy connector degassed for 30 minutes at 2500Pa. As the connector was filled outside of vacuum, there may have been air present or trapped in the resin epoxy during filling. The proxy connector was left to harden over 48 hours, before the shut-off plate was removed.

Micro-CT scanning of the connector:

The connector was then taken to the Micro-CT system (Nikon XT H 225 ST) at Flinders University's Tonsley campus (Wearne et al., 2022), where it was scanned with voxel resolutions of 38µm and 24µm to check for any voids or irregularities within the epoxy. Source voltage was 215kV, source current was 112µA, and a 0.25mm tin filter was used.

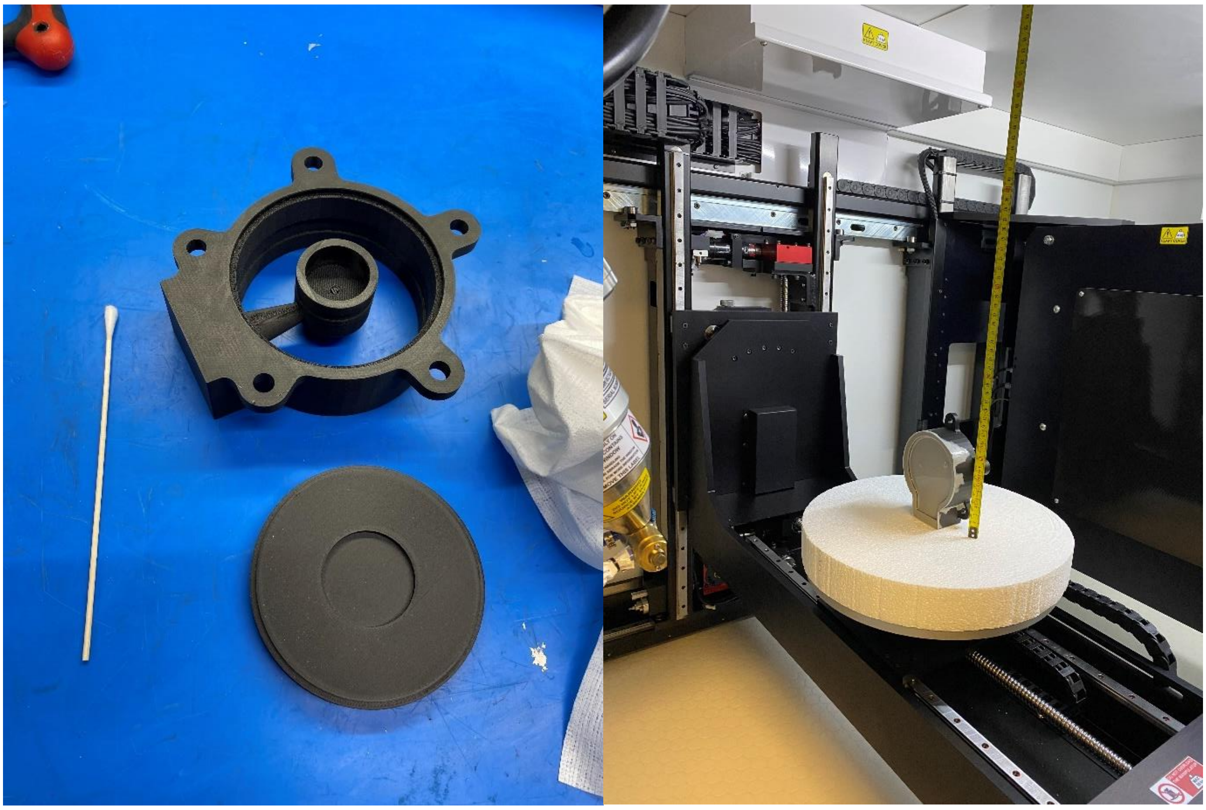

Figure 14 – The proxy connector and shut-off plate (left) and the encapsulated connector ready for scanning inside the Micro-CT, standing upright on the sample holder (right).

It was determined from the above experiments that an active cooling solution for the connector shut-off plate was unnecessary, and that simply pouring the resin epoxy into the connector slowly is adequate for preventing voids and bubbles from pouring during the curing process, as described by Bolon (1995). Degassing the connector after potting did, however, result in some overflow and bubbles appearing on the open surface of the connector. Further elaboration can be found in the Results and Discussion sections.

Design and manufacture of the connector:

Using Solidworks (2019), a connector and potting aids were designed. There were six components in total: the main body of the connector, centre conductor pin, a covering plate, a shut-off plate, a cable earthing interface, and finally a main body extrusion. Using Agros, an electric field simulator, the cable connector was analysed to check for areas of high stress and the connector modified if these were present. After 3D printing the connector body to test compatibility, the components were manufactured out of 6061 alloy aluminium by Absolute Engineering Solutions (Lonsdale, SA) except for the main body extrusion, which was 3D printed at Micro-X. The shut-off plate was treated with a non-stick coating of PFA by Dixon Industries Pty Ltd (Royal Park, SA) to ensure it could be removed from the assembly after potting. Various fasteners were obtained from RS Components, and O-rings from BSC Lonsdale.

The rear cover plate (*Connector cover*, Micro-X part number 27744) was the simplest component of the connector assembly; a 3mm thick part that matches the profile of the main connector body (*Anode cable connector body*, Micro-X part number 27745). The connector body has an internal diameter of 85mm, to attach correctly to the Cooper generator output interface. The external fastener positions have clearance for M8 threads to pass through, and are spaced at either 70°, 72°, or 74° intervals relative to each other so that the fastener holes align with those on the Cooper generator. There is a port for the high voltage cable to pass through, with M3 threaded holes for attachment of the earthing interface. The centre conductor pin (*Centre pin*, Micro-X part number 27748) has an external diameter of 35mm, with an internal diameter of 27.5mm, again to attach correctly to the Cooper generator. It also features a centred M2 thread for attachment of a male banana pin. Adjacent to this pin are two M4 threads, which hold the centre pin firmly against the shut-off plate during curing. Finally, an untapped hole on the side allows for insertion of the high-voltage cable, held in place by an M2 grubscrew threaded in from the underside.

The cable earthing interface (*Cable earthing interface,* Micro-X part number 27749), allows the metal sheath of the high-voltage cable to be held in place, as well as providing further mechanical support to the rest of the connector. There is room for an O-ring between it and the main body to prevent resin epoxy from leaking around the cable during curing. The shut-off plate (*Pull off plate for anode cable connector,* Micro-X part number 27750) is one of the more complex pieces, designed to fit snugly within the main body, as well as hold the centre pin firmly in place. It has five clearance holes for M8 threads in the same orientation as those on the main body; this is where the components are fastened together. Additionally, it has a 3mm raised surface which sits flush on an inner ring inside the main connector body. This 3mm raised surface has a groove for a 1mm thick x 90mm outer diameter O-ring to be fitted, and on the inner surface a similar groove for a 1mm thick by 35mm inner diameter O-ring to prevent leakage around the main body and centre pin respectively. This inner section also has clearance holes for M4 threaded fasteners to pass through, allowing for the centre pin with tapped threads to be held in place. The part also has a layer of non-stick PFA applied after manufacture. Mechanical drawings and images are found in the appendix (figure 27).

Cleaning of the connector and preparation for potting:

The aluminium components that would contact resin epoxy were cleaned in the Micro-X clean room. This process involved scrubbing the components with 10% Citranox solution with electric scrubbing brushes and pipe brushes. The components were then rinsed with cold distilled water to remove lingering Citranox solution before being thoroughly steam cleaned with distilled water. The components were rinsed once again with distilled water before undergoing a rinse using isopropyl alcohol. Nitrogen was used to blow off excess liquid before the components were placed into a drying oven at 150 degrees for 30 minutes. This process follows the Micro-X document STS304 *Cooper Component Cleaning* guidelines. A high-voltage cable (Varex U3 specification) with one end terminating in a Varex R24 connector for Spellman generator compatibility was stripped and the bare inner conductors soldered together. The rubber insulating layer was then tapered using a sharp knife to ease electric field stresses, as demonstrated by Illias et al. (2012) and Raicevic (1999). If the cable was interfaced to the centre conductor pin directly electric field stresses would amplify at this boundary; thus a taper is necessary to ‘bend’ the electric field equipotential lines along the cable to result in lower stresses (Malik et al., 2010).

O-rings were fitted onto the shut-off plate where it would interface with the centre conductor pin and the main connector body, as well as between the main body and the earthing interface. The connector was assembled with the shut-off plate at the bottom, and the high voltage cable inserted into the centre conductor pin, where a grubscrew held it in place. The metal sheath of the cable (acting as the ground conductor) was pulled over the connector's earthing interface component and fastened in place using a large crimp. Additionally, solder was applied to further increase the bond between the cable sheath and the aluminium of the connector. The 3D printed extrusion was fastened to the top of the connector, and electrical tape applied to help seal the gap between the two.

Figure 15 – The connector being assembled (left), featuring the shut-off plate, main body, and conductor pin. The right image includes the cable, cable interface, tape, and extrusion.

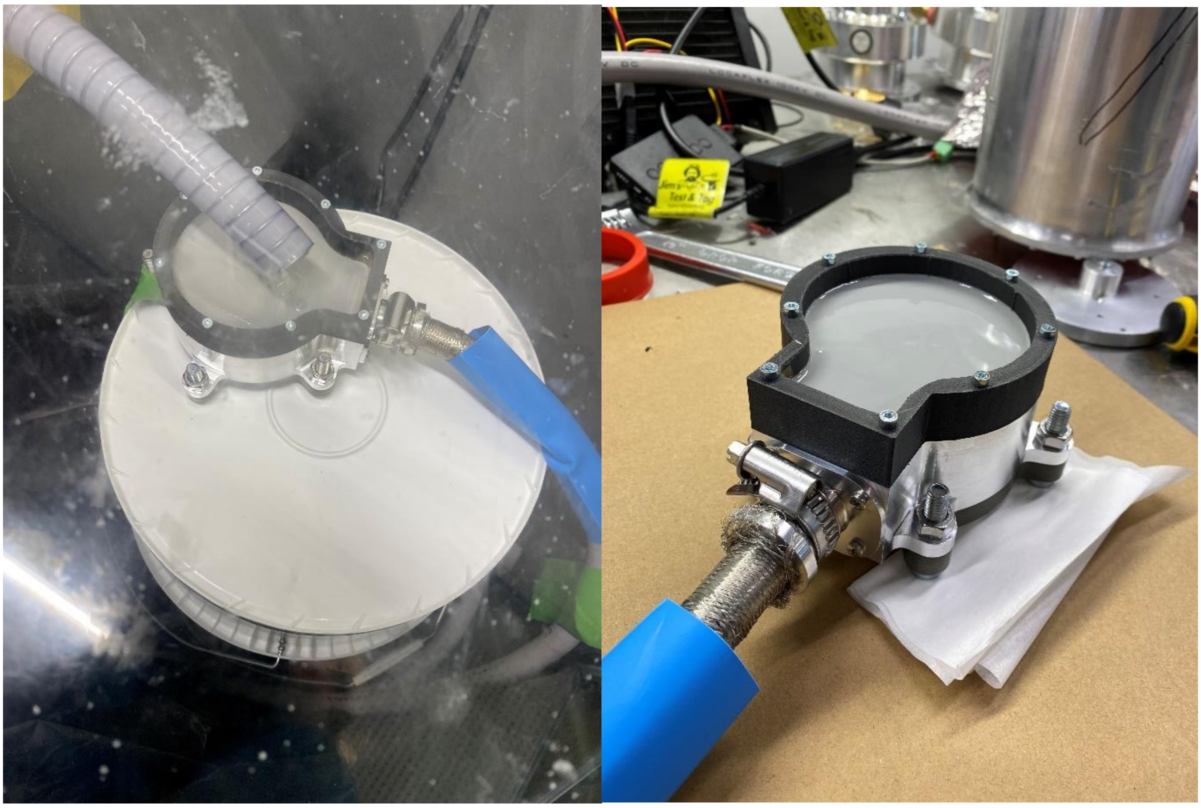

Figure 16 – Potting the connector in a vacuum chamber (left) and curing it on a flat surface.

Potting of the connector:

The connector assembly was then transferred to a vacuum chamber. “Megapoxy E Slow” resin epoxy was prepared as per STS314 *Potting Material Preparation*, previously described in the Dielectric strength testing of epoxy section of this thesis. However, unlike the 3D printed proxy connector, the epoxy was mixed and the connector assembly potted entirely under vacuum. The connector was placed flat atop a bucket inside the vacuum chamber. A pipe was cut to size so that resin entering the chamber will flow into the connector from above, pouring the epoxy as per Bolon (1995). Pressure inside the vacuum chamber was 2500Pa before the epoxy was allowed to flow slowly into the pressure chamber and then the connector. Filling was slow (approximately 2 minutes) to prevent turbulence, and the connector was held under vacuum for an additional 10 minutes as this reduces void content as outlined by Tang et al. (1987). The connector was left to cure over 72 hours.

After 72 hours, the shut-off plate was removed, revealing a perfectly smooth connector interface. However, the excess hardened epoxy and 3D printed extrusion were required to be machined off by Absolute Engineering Solutions (Lonsdale, SA). Small voids were noted on the area where the excess epoxy had been removed; these were visually determined to be damage from the machining process and not voids from the potting process. The largest voids were approximately 5mm in size, and their boundaries aligned with the path taken by the machining bit. Additionally, these voids did not glisten or shine like voids that occur during curing have been observed to do at Micro-X. These voids were patched up by syringing small amounts of resin epoxy onto them at the next opportunity, before being sanded down to an acceptably smooth finish. This process has been used at Micro-X before to fix small voids on critical surfaces (such as the connector interface), and so is appropriate for use on the backside of the connector. After fixing this side of the connector, a small amount of silicon dielectric grease was applied to prevent air ingress, and the connector cover fastened to the connector. A continuity test was performed on the connector, and the two conductors were not in a short circuit.

Testing of the potted connector and anode cable assembly:

A Spellman “SLM” generator capable of producing up to 160kV was obtained, and the R24 connector half the cable inserted into its high-voltage output. Unfortunately, this generator was unavailable for testing the epoxy samples as outlined previously. The potted connector was interfaced to a blanking plate; simply a block of epoxy with a Cooper generator interface that ensures an open circuit between the conductor and ground. A withstand test was performed on the connector, again applying a ramp pulse of 1kV/second through the connector until 120kV was reached, at which point the voltage was applied for another 60 seconds. Then, testing was performed in accordance with IEC 60601 *Medical Electrical Equipment*. This standard calls for a test voltage 1.2x the nominal voltage be applied; as the Rover tubes operate at 110kV the test voltage was 132kV. Half the test voltage (66kV) was applied to the connector, ramping up to 132kV over 10 seconds before holding at 132kV for an additional 3 minutes as per the standard. The current limit was set to 5mA, the maximally allowed value of earth leakage current for mobile X-ray equipment.

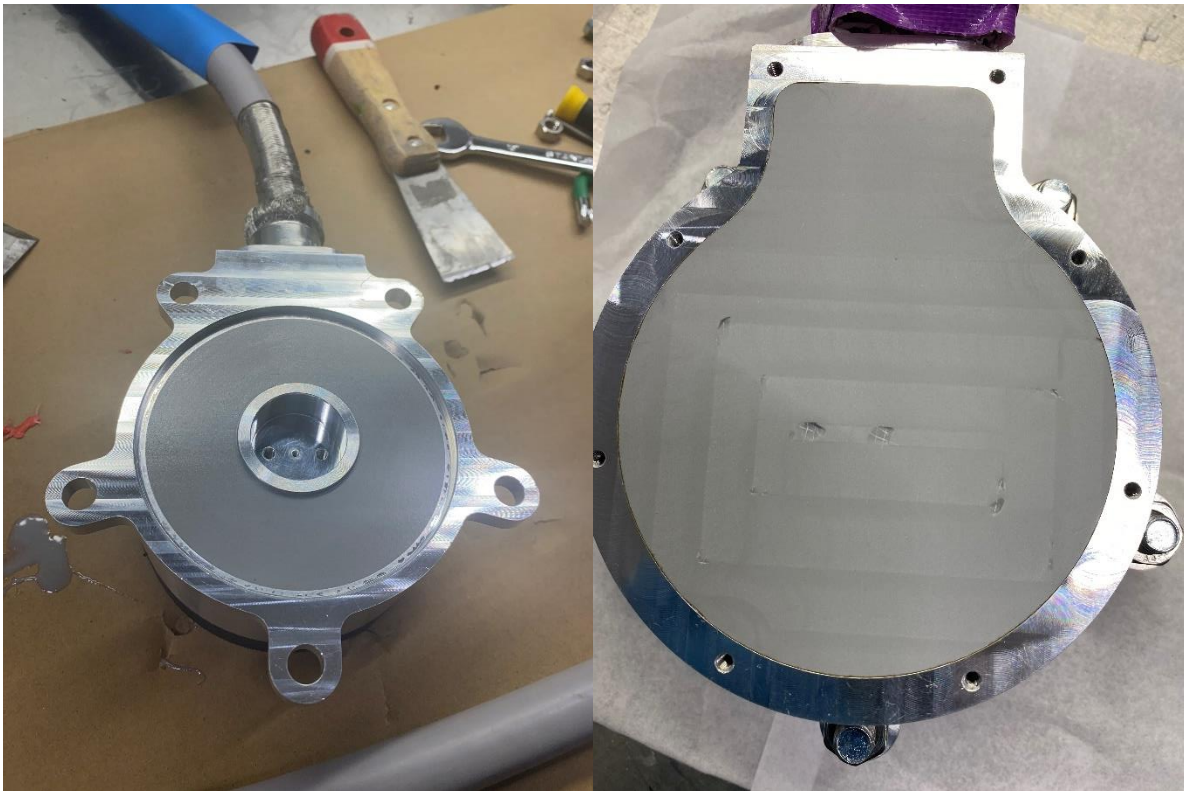

Figure 17 – A successful pot (left) and the backside of the connector showing minor damage after machining off the excess epoxy (right). Note the position and shape of the voids align with the tracks of the machining bit. Additional images in the appendix (figure 28).

Accelerated life testing with 110kV step pulses was then performed on the connector. The applied voltage pulses were identical to those applied to the epoxy samples previously (2 seconds at max voltage, 4 seconds off) but at 110kV rather than 120kV.

Results (Aim 1) – Dielectric strength testing of epoxy with different alumina nanofiller concentrations:

Neat epoxy:

All four neat epoxy samples survived the initial ramp pulse, and only failed during accelerated lifespan testing (tables 1 and 2). Of these, one sample failed after 36 pulses, the other three samples failed after 486, 593, and 609 pulses, for an average of 431 pulses (n=4). As all four samples survived the initial withstand test, no breakdown voltage could be determined.

Epoxy with nanofillers:

Of the 0.5% concentration samples, only one survived the initial ramp pulse, but failed during the first ALT pulse it was subjected to. The other three samples failed at 117kV, 113kV, and 86.7kV. Thus, the samples survived an average of 0.25 ALT pulses before failure (n=4). The 1% samples all survived the initial ramp pulse, and broke down after 10, 49, 229, and 64 cycles, providing a mean of 88 cycles (n=4). Of the 2% samples, one failed during the hold portion of the withstand test, having survived the ramp portion. The three samples that survived into ALT testing broke down after 14, 49, and 253 cycles, for a mean of 79.25 cycles (n=4, Fig. 18). Again, as all samples survived the withstand test, no breakdown voltage was determined for the 1% and 2% concentrations.

The two samples of “Megapoxy E Slow” that were mechanically mixed under vacuum (unlike all other samples, which were hand-mixed in air) did not experience breakdown, even after 21,900 cycles.

Table 1 – Withstand test: voltage at which breakdown occurred during ramping to 120kV, for each sample for each group of concentration of nanofillers

Sample number	Neat	0.5% Al_2O_3	1% Al_2O_3	2% Al_2O_3
1	No breakdown	117.2 kV	No breakdown	No breakdown
2	No breakdown	No breakdown	No breakdown	No breakdown
3	No breakdown	113.9 kV	No breakdown	No breakdown
4	No breakdown	86.7 kV	No breakdown	No breakdown

Table 2 – Accelerated life time (ALT) test: number of pulses (120kV step pulses) experienced by each sample before breakdown, with average and standard deviation (SD) for each group.

Sample number	Neat	0.5% Al_2O_3	1% Al_2O_3	2% Al_2O_3
1	486	0	10	1
2	36	1	49	14
3	593	0	229	253
4	609	0	64	49
Average (SD)	431 (269)	0.25 (0.5)	88 (97)	79 (118)

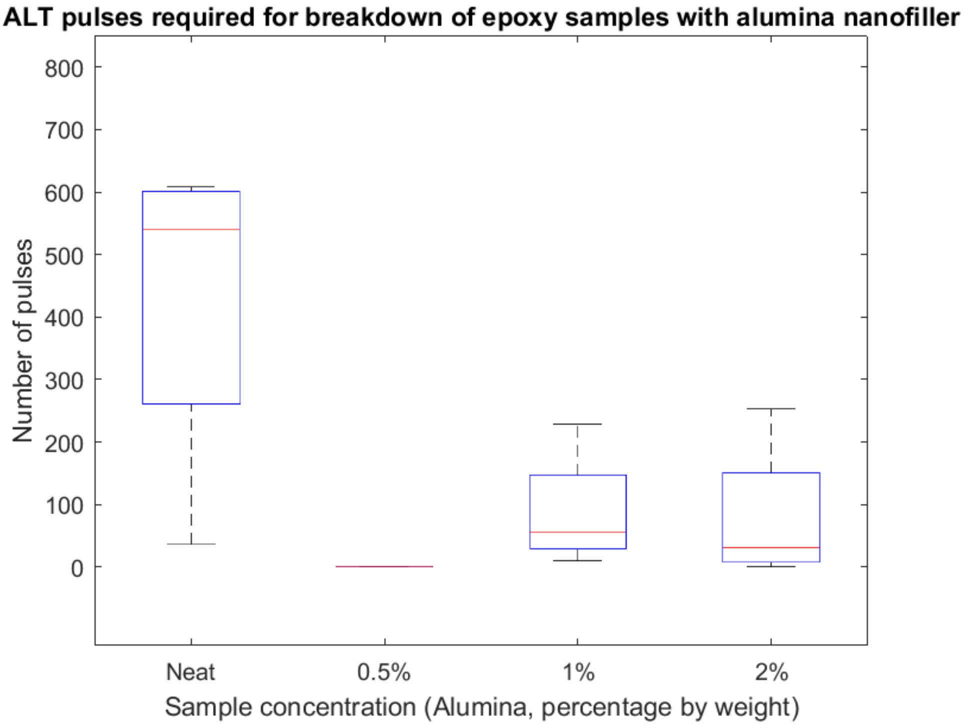

Figure 18 – Number of accelerated lifespan test pulses required before dielectric breakdown of epoxy samples was recorded. For each concentration, number of samples = 4. Red line: the mean for each concentration; blue box: 25th to 75th percentiles; error bars the minimum and maximum values.

The Kruskal Wallis test performed on the number of ALT pulses before breakdown showed that there were significant differences among the groups ($p < 0.0155$). Following this, a Mann Whitney test was conducted, comparing each of the filled epoxy groups (0.5%, 1% and 2%) to the neat group. The 0.5% alumina nanocomposite had a significantly lower number of pulses compared to neat group ($p = 0.0286$). The 1% and 2% group showed a trend to have a lower number of pulses than the neat, although not statistically significant ($p = 0.2000$ and 0.1143, respectively).

Partial breakdown:

Most tests did not record any partial discharge events; however, the Picoscope was able to detect the full breakdown of all samples. The second sample of 2% Al_2O_3 nanofiller (which survived 14 cycles) experienced what may have been a partial discharge event during its second ALT pulse, with the Picoscope logging 9MB of data.

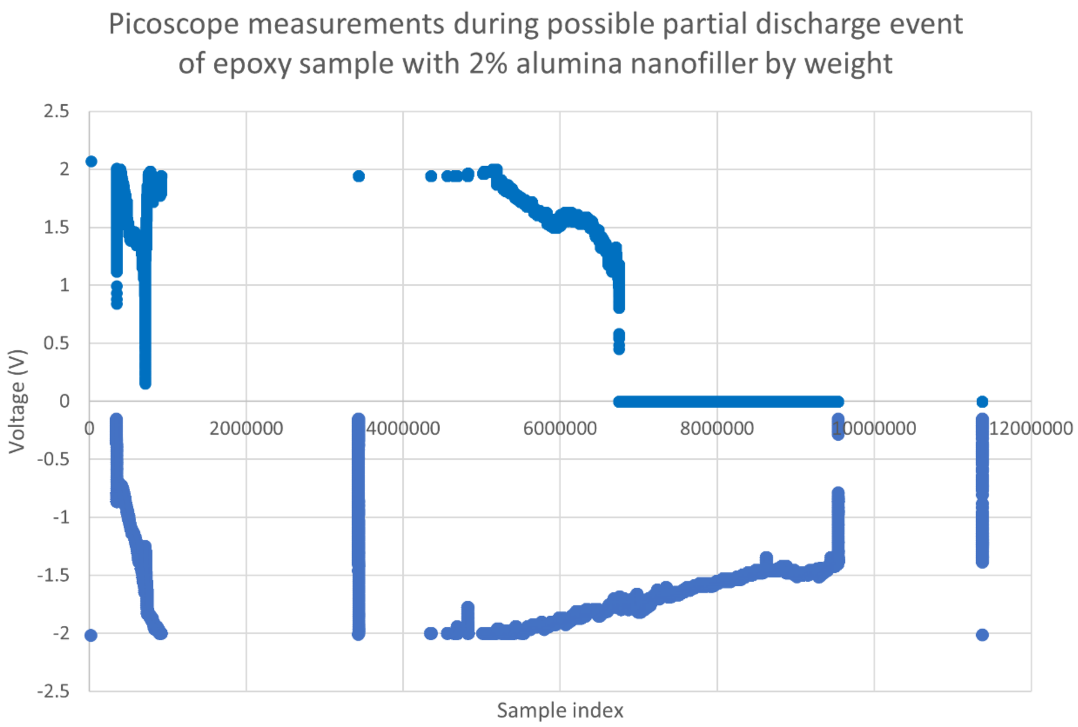

Figure 19 – Picoscope measurements during possible partial breakdown event for 2% nanofiller sample number 2, which survived 14 cycles total. Generated in Microsoft Excel.

Results (Aim 2) – Design and encapsulation of high-voltage connector:

The initial temperature measurements yielded by the Arduino and Python scripts showed a temperature delta of about 5.5 °C above ambient at the maximum, which occurred about an hour after initial potting.

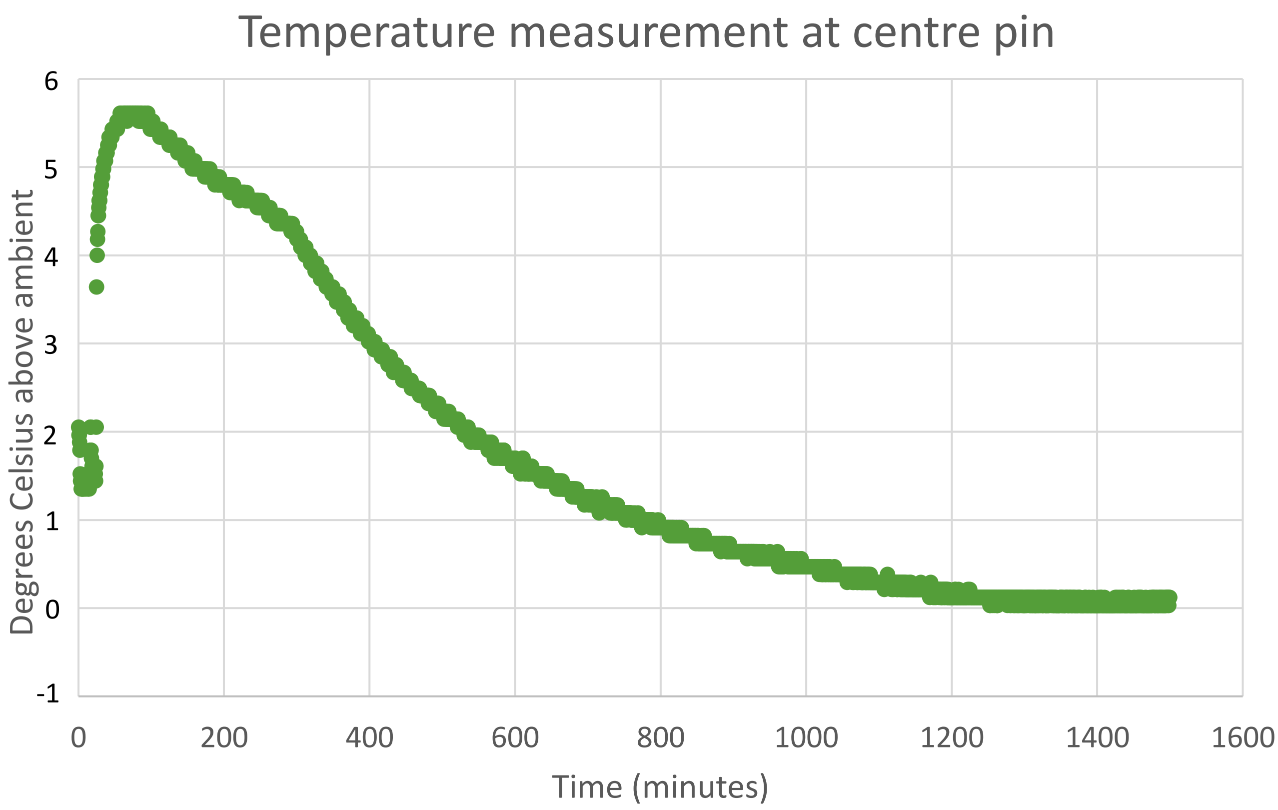

Figure 20 – The first 15 hours of temperature measurement as recorded by the Arduino using a thermistor at the centre pin of a 3D printed proxy connector during curing. Generated in Microsoft Excel.

The micro-CT cross-section images of the potted 3D printed proxy connector showed no visible voids present in the entirety of the potted volume, apart from only a few surface bubbles. These bubbles were small and only a few hundred µm in diameter at their maximum. Most were only a few pixels across, barely over 100 µm. Cross-section images can be found in the appendix (Fig. 26).

The cable connector was successfully potted using Micro-X's potting techniques; the epoxy surface covered by the shut-off plate was smooth and the centre pin aligned correctly. Dry fitting the connector onto a Cooper generator as well as an X-ray tube was successful, and continuity tests performed with a multimedia showed there were no short circuits between conductors, and that conductor integrity was satisfactory.

Successful IEC testing and X-ray imaging:

The potted cable connector assembly passed testing as per IEC 60601 *Medical Electrical Equipment,* able to withstand an applied 132kV for 3 minutes after a 10 second ramp up from 66kV. No corona discharges were observed (although their presence does not necessarily result in failure), and no leakage current was detected by the Spellman generator. The cable was then interfaced to an X-ray tube, and an image of a watch produced (Fig. 22). After the image was produced, then cable assembly was subjected to 21,900 ALT pulses at 110kV; during this time no arcs or leakage currents were detected. As of time of writing, the connector assembly had survived over 30,000 ALT pulses – a year and a half of heavy use, at 110kV as described in the Methods section of this thesis.

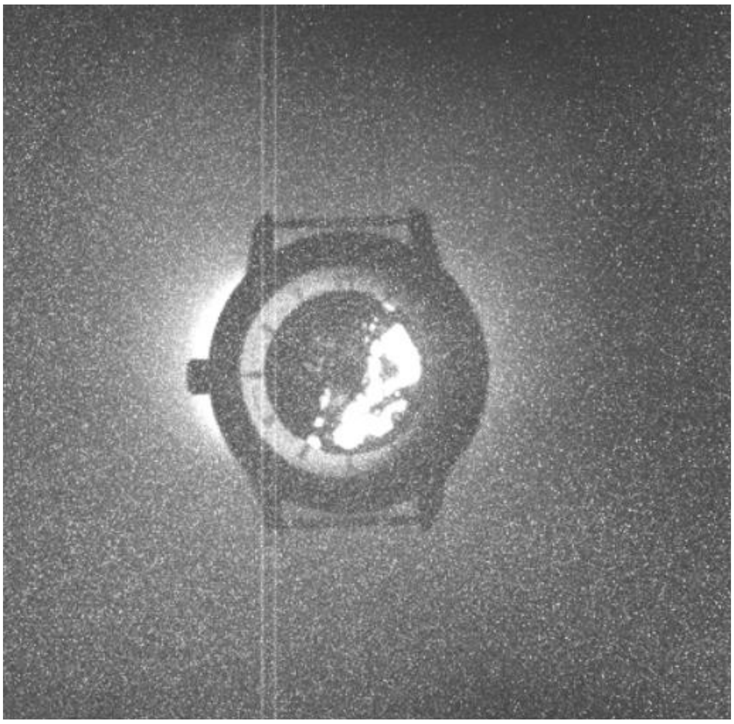

Figure 21 – X-ray of a watch produced using a CNT X-ray tube powered by the potted anode cable. X-ray settings: 55kV, 20mA with 5 seconds of exposure.

Discussion:

Dielectric strength testing of epoxy with different Al_2O_3 nanofiller concentration (Aim 1):

Alumina oxide nanofillers, when added to bisphenol-A based epoxy, had a profound effect on the dielectric strength of the resulting nanocomposites. When compared to neat epoxy, which was able to survive hundreds of ALT pulses, nanocomposites containing 0.5% Al_2O_3 by weight underperformed, with only one able to survive the initial withstand test. This was statistically significant ($p = 0.0286$). An average breakdown voltage can be deduced for the failed samples of this concentration, at 105.95 kV/ 3mm (sample thickness) which equates to 35.32 kV/mm. The differences between neat epoxy and 1% or 2% samples are not statistically significant, however, a trend can be observed that the groups with nanofiller still performed more poorly compared to the neat (Fig. 18). The tests for concentrations other than 0.5% did not return a "breakdown voltage" value; an estimate to the amount of electric field stress (kV/mm) that should cause dielectric breakdown of epoxy samples, as most samples survived the initial ramp pulse. Rather, the significant differences in the mean number of ALT pulses survived by each concentration show that there is indeed a difference in their dielectric strengths, but not one that can be simply quantified into a breakdown voltage.

These results most closely reflect those of Singha and Thomas (2008), in that adding Al_2O_3 nanofiller to bisphenol-A based epoxy decreased the breakdown voltage of the epoxy. Here, adding **alumina** nanofiller to epoxy resulted in a decrease to the amount of ALT pulses each sample could withstand, relating to the dielectric strength of the material. Interestingly, Singha and Thomas's results showed that the magnitude of this effect increased with increased nanofiller concentration, whereas the results of this thesis show only an increased variance between samples (Fig. 18). This phenomenon more closely reflects the work of Mohanty and Srivastava (2013), who showed an increase in the breakdown voltage of epoxy with an increase in Al_2O_3 nanofillers, up to 4%, after which the effect reversed. However, the results of these experiments are in direct opposition to Andritsch et al. (2010), whose experiments saw the best results compared to neat epoxy with 0.5% nanofiller samples. The variation in results may be from the dispersal of nanoparticles in the epoxy samples; Mohanty and Srivastava observed poorer dispersion of nanoparticles and some aggregations at higher concentrations. Andritsch did not report on their dispersal, Singha and Thomas noted uniform dispersal. Due to time constraints, the dispersal of nanofillers within the samples tested in this thesis were not determined in this thesis. Dispersal can been quantified using a scanning electron microscope, as shown by Omrani et al. (2009), Ho et al. (2006), and Preetha and Thomas (2011).

Partial discharges were not detected in these tests. It is generally accepted that partial discharge events, if present, increase in either frequency or magnitude preceding full dielectric breakdown of insulation materials (Niemeyer, 1995). The aging of materials is also crucial in the prediction of partial discharge events; it is likely that the samples produced for the tests in this thesis simply experienced dielectric breakdown during the first ‘partial’ discharge. Should the samples have been of higher dielectric strength, then partial discharge events may have been more prevalent prior to a breakdown. It is also possible that the Picoscope was unable to detect minute partial discharges, these could also have acted like leakage currents and not have travelled through the earth wire. Moreover, the single log file generated by the Picoscope (Fig. 20) is not particularly useful, as there are multiple data points per index as well as clipping for voltages with a magnitude greater than 2V. Visually, the shape of the graph does not reflect the literature, which usually portrays a sharp transient followed by oscillating decay (Okubo and Hayakawa, 2005).

Design and encapsulation of high-voltage connector (Aim 2):

Air bubbles were present on the surface of all samples potted in air (appendix, Fig. 23), which almost certainly decreased the dielectric strength of the epoxy samples. However, the bubbles appeared not to vary too much between samples in both frequency and size, indicating that systematic error had minimal effect on the outcome of these experiments. The “Megapoxy E Slow” samples that were mixed and potted under vacuum, each survived 21,900 ALT pulses before testing was stopped on them; these samples exhibited no external bubbles. This provides indirect evidence that voids or bubbles present on the surface of cured epoxy will amplify electric field stresses.

There were some observable resolution issues with the temperature data obtained during curing of the 3D printed proxy connector as can be seen in appendix Fig. 22, and the temperature appears to clip at its maximum point. Additionally, at about the 5-hour mark, the slope of the temperature appears to change. However, this test did not require a high accuracy in measurement, rather simply to determine if it was required to design an actively cooled shut-off plate when potting the connector. The micro-CT scans were helpful in excluding possible internal pores (appendix, Fig. 26), which were shown to be present mainly on the surface. This is in line with Micro-X having been using this brand of epoxy for years, observing that it penetrates gaps 0.1mm wide.

IEC 60601 *Medical Electrical Equipment* standard:

The connector itself was designed and potted well enough to pass the tests as set out in the IEC 60601 *Medical Electrical Equipment* standard, as well as survive thousands of ALT pulses at it the nominal voltage it would be operating at. The Micro-X potting process it seems is appropriate for potting small volumes such as the cable connector, and such small volumes do not achieve a high enough exotherm to be concerned about pull-away or shrinkage during curing.

There were several limitations observed during the undertakings of this thesis; the chief among them that the epoxy samples were limited to at most a 40kV/mm electric field stress. This was due to the Spellman ST generator used for these tests only being capable of generating 120kV, and the electrode moulds that were used ensured the electrodes were 3mm apart. Using a more powerful generator or redesigning the moulds to bring the electrodes closer would allow for higher stress to be exerted on the epoxy samples, perhaps allowing a more significant ramp pulse to be applied and a true breakdown voltage value determined. Secondly, the mixing of the resin epoxy had to be done by hand, exposing the resin to both air and possible contaminants. This was not true for the “Megapoxy E Slow” samples mixed and potted under vacuum, and they were the only samples to survive the full

21,900 ALT pulses. There were also only 4 samples at each concentration due to the lengthy resin epoxy preparation and curing times, as well as only two electrode moulds available for use. Should time and resources have not been a factor, significantly more samples at each concentration would have been produced so that the results carry more weight. This would also have the advantage of ensuring each sample came from the same batch of epoxy, reducing variation between samples of the same nanofiller concentrations. The nanofiller concentrations were not verified to confirm the manufacturer labelled them correctly.

To account for the limited sample size, non-parametric statistical tests (Kruskal Wallis and Mann-Whitney tests) were used for statistical comparisons, rather than parametric tests. Nonetheless, statistically significant differences were observed between the neat epoxy and the 0.5% concentration samples.

Conclusions:

The experiments in this thesis show that adding low concentrations of aluminium oxide nanofillers to bisphenol-A based resin epoxy may decrease the DC dielectric strength of the nanocomposite compared to neat epoxy. This effect was shown here to only be statistically significant at concentrations of 0.5% by weight. For all nanocomposites except for 0.5% Al_2O_3 by weight, no breakdown voltages of these nanocomposites were determined. It was found that nanocomposites with this level of Al_2O_3 nanofiller will likely experience dielectric breakdown when a DC voltage gradient greater than 35.32 kV/mm is applied across it. Partial discharge data preceding dielectric breakdown of the samples was non-existent and cannot be commented upon.

A high-voltage anode cable connector for use in mobile X-ray devices was designed and manufactured, then potted using Micro-X's potting process which had previously not been tested on small volumes. The potting technique is adequate for small volumes and does not result in detectable voids or bubbles in the body of the cured product (some may be present on the surface), nor is an active cooling solution required as with larger volumes. The anode cable connector passed the dielectric strength requirements set out by IEC 60601 *Medical Electrical Equipment* as well as thousands of ALT pulses replicating years of heavy use, and sets the precedent for future potting of smaller volumes at Micro-X.

Future work:

First, the previous nanocomposite samples should be scanned using a SEM to check for filler size, dispersion, and for aggregates. Results of the scans can then be compared to the literature to determine if the dispersion has a marked effect on the dielectric strength of the nanocomposites. Micro-CT scans could also be performed of the epoxy between the electrodes, not only to determine if the electrodes bonded properly, but also if there were any voids present before and after breakdown. Perhaps the size of voids, if any, may increase over time, due to electric treeing. Repeating the experiments but potting the electrodes entirely as per the Micro-X potting process (under constant vacuum whilst mixing, potting, and curing) would also strengthen the outcome of this thesis, as then the effect of bubbles would be minimised, and any deviations in dielectric strength caused purely by the nanoparticle concentration and dispersion.

Regarding the connector design, some teething issues were noted by the author; it was quite difficult to remove the shut-off plate from the connector after curing, even though it had been coated in PFA (non-stick coating). The electrode moulds feature threaded holes that fasteners could be inserted into to 'crack' open the moulds, future iterations of the shut-off plate and connector should incorporate something similar. Additionally, there are no commercially available O-rings 1mm thick with an inner diameter of 88mm, instead, 1mm x 90mm O-rings had to be cut to size which risks leaks or the O-ring breaking. Again, future iterations of the connector and shut-off plate should incorporate these, or a supplier found that can manufacture O-rings of this size. This potting technique has now been validated for small volumes, and the miniaturisation of components such as high-voltage generators is avenue Micro-X can begin to explore.

Bibliography

ADNAN, M. M., TVETEN, E. G., GLAUM, J., ESE, M. H. G., HVIDSTEN, S., GLOMM, W. & EINARSRUD, M. A. 2019. Epoxy-Based Nanocomposites for High-Voltage Insulation: A Review. *Advanced Electronic Materials,* 5**,** 1800505.

AFENDI, M., BANKS, W. M. & KIRKWOOD, D. 2005. Bubble free resin for infusion process. *Composites Part A: Applied Science and Manufacturing,* 36**,** 739-746.

AMIN, M., KHATTAK, A. & ALI, M. 2016. Life estimation and investigation of dielectric strength of multistressed high-voltage epoxy micro and nanocomposites. *Micro & Nano Letters,* 11**,** 765-768.

ANDRITSCH, T., KOCHETOV, R., MORSHUIS, P. H. & SMIT, J. J. Short term DC breakdown and complex permittivity of Al 2 O 3-and MgO-epoxy nanocomposites. 2010 Annual Report Conference on Electrical Insulation and Dielectic Phenomena, 2010. IEEE, 1-4.

ARNS, R. G. 1997. The high-vacuum X-ray tube: technological change in social context. *Technology and Culture,* 38**,** 852-890.

ARORA, R. & MOSCH, W. 2022. *High voltage and electrical insulation engineering*, John Wiley & Sons.

AWAJA, F., ARHATARI, B., WIESAUER, K., LEISS, E. & STIFTER, D. 2009. An investigation of the accelerated thermal degradation of different epoxy resin composites using X-ray microcomputed tomography and optical coherence tomography. *Polymer Degradation and Stability,* 94**,** 1814-1824.

AZIZIAN FARD, M., FARRAG, M. E., REID, A. & AL-NAEMI, F. 2019. Electrical treeing in power cable insulation under harmonics superimposed on unfiltered HVDC voltages. *Energies,* 12**,** 3113.

BABU, M. S., SARATHI, R., VASA, N. J. & IMAI, T. 2019. Understanding the influence of nano micro filler on electrical and mechanical behaviour of epoxy nanocomposites. *IEEE Transactions on Dielectrics and Electrical Insulation,* 26**,** 1098-1106.

BALACHANDRAN, M., VISWAKUMAR, K. & NAMBIAR, T. 2017. Modeling of electric field distribution in epoxy nanocomposites using Finite Element Method. *Journal of Electrical Engineering,* 15.

BECKER, O., CHENG, Y.-B., VARLEY, R. J. & SIMON, G. P. 2003. Layered Silicate Nanocomposites Based on Various High-Functionality Epoxy Resins: The Influence of Cure Temperature on Morphology, Mechanical Properties, and Free Volume. *Macromolecules,* 36**,** 1616-1625.

BERGER, L. 2006. Dielectric strength of insulating materials. *Carbon,* 1**,** 2.

BERO, C. A. & PLAZEK, D. J. 1991. Volume-dependent rate processes in an epoxy resin. *Journal of Polymer Science Part B: Polymer Physics,* 29**,** 39-47.

BOLON, D. A. 1995. Epoxy chemistry for electrical insulation. *IEEE Electrical Insulation Magazine,* 11**,** 10-18.

BOONE, J. M. 2000. X-ray production, interaction, and detection in diagnostic imaging. *Handbook of medical imaging,* 1**,** 1-78.

BURM, K. T. A. L. 2007. Calculation of the Townsend Discharge Coefficients and the Paschen Curve Coefficients. *Contributions to Plasma Physics,* 47**,** 177-182.

CHANG, J., LAWLESS, P. A. & YAMAMOTO, T. 1991. Corona discharge processes. *IEEE Transactions on Plasma Science,* 19**,** 1152-1166.

CHEKANOV, Y. A., KOROTKOV, V., ROZENBERG, B., DHZAVADYAN, E. & BOGDANOVA, L. 1995. Cure shrinkage defects in epoxy resins. *Polymer,* 36**,** 2013-2017.

CHENG, Y., YU, G., ZHANG, X. & YU, B. 2020. The research of crystalline morphology and breakdown characteristics of polymer/micro-nano-composites. *Materials,* 13**,** 1432.

DEBERTIN, K. & HELMER, R. G. 1988. Gamma-and X-ray spectrometry with semiconductor detectors.

FUJITA, S., RUIKE, M. & BABA, M. Treeing breakdown voltage and TSC of alumina filled epoxy resin. Proceedings of Conference on Electrical Insulation and Dielectric Phenomena - CEIDP '96, 23-23 Oct. 1996 1996. 738-741 vol.2.

GHOUSE, S. M., VENKATESH, S., RAJESH, R. & NATARAJAN, S. 2013. Effects of SiO2 and TiO2 nano fillers in enhancing the insulation breakdown strength of epoxy nano composite dielectric under divergent electric fields. *International Journal on Electrical Engineering and Informatics,* 5**,** 501.

GONZALES, B. 2020. *X-Ray Imaging: Introduction to CNT emitter technology and life testing* [Online]. Available: https://micro-x.com/wp-content/uploads/2021/07/ROV224-02-CNT-Life-White-Paper-27072021.pdf [Accessed 18/03/2022 2022].

HADDAD, A., HADDAD, M., WARNE, D. & WARNE, D. 2004. *Advances in high voltage engineering*, IET.

HASEGAWA, B. H. 1990. The physics of medical x-ray imaging.

HO, M.-W., LAM, C.-K., LAU, K.-T., NG, D. H. L. & HUI, D. 2006. Mechanical properties of epoxy-based composites using nanoclays. *Composite Structures,* 75**,** 415-421.

HOGG, M. G., TIMOSHKIN, I. V., MACGREGOR, S. J., WILSON, M. P., GIVEN, M. J. & WANG, T. Electrical breakdown of short non-uniform air gaps. 2013 19th IEEE Pulsed Power Conference (PPC), 16-21 June 2013 2013. 1-4.

HOLTZHAUSEN, J. & VOSLOO, W. 2014. High Voltage Engineering Practice and Theory. *Stellenbosch, Western Cape*.

HUGHES, A., MAYO, S., YANG, Y., MARKLEY, T., SMITH, S., SELLAIYAN, S., UEDONO, A., HARDIN, S. & MUSTER, T. 2012. Using X-ray tomography, PALS and Raman spectroscopy for characterization of inhibitors in epoxy coatings. *Progress in Organic Coatings,* 74**,** 726-733.

HUSAIN, E. & NEMA, R. 1982. Analysis of Paschen curves for air, N2 and SF6 using the Townsend breakdown equation. *IEEE transactions on electrical insulation***,** 350-353.

ILLIAS, H. A., NG, Q. L., BAKAR, A. H. A., MOKHLIS, H. & ARIFFIN, A. M. Electric field distribution in 132 kV XLPE cable termination model from finite element method. 2012 IEEE International Conference on Condition Monitoring and Diagnosis, 23-27 Sept. 2012 2012. 80-83.

IMAI, T., SAWA, F., OZAKI, T., INOUE, Y., SHIMIZU, T. & TANAKA, T. Comparison of Insulation Breakdown Properties of Epoxy Nanocomposites under Homogeneous and Divergent Electric Fields. 2006 IEEE Conference on Electrical Insulation and Dielectric Phenomena, 15-18 Oct. 2006 2006. 306-309.

IYER, G., GORUR, R., RICHERT, R., KRIVDA, A. & SCHMIDT, L. 2011. Dielectric properties of epoxy based nanocomposites for high voltage insulation. *IEEE Transactions on Dielectrics and Electrical Insulation,* 18**,** 659-666.

KARA, A., Ö, K. & MARDIKYAN, K. DC breakdown voltage characteristics of small air gaps with insulating barriers in non-uniform field. 2010 International Conference on High Voltage Engineering and Application, 11-14 Oct. 2010 2010. 425-428.

KHOUN, L. & HUBERT, P. 2010. Cure shrinkage characterization of an epoxy resin system by two in situ measurement methods. *Polymer composites,* 31**,** 1603-1610.

KIND, D. & KÄRNER, H. 1985. *High-voltage insulation technology*, Springer.

KITICHATPAYAK, D., MAKCHAROEN, W., VITTAYAKORN, N. & VITTAYAKORN, W. 2022. Influence of various nanofillers on mechanical and electrical properties of epoxy resin composites. *Polymer-Plastics Technology and Materials***,** 1-7.

KOCHETOV, R., TSEKMES, I. A., CHMURA, L. A., MORSHUIS, P. H. F., IIZUKA, T., TATSUMI, K. & TANAKA, T. The effect of nanosilica on the DC breakdown strength of epoxy based nanocomposites. 2014 IEEE Conference on Electrical Insulation and Dielectric Phenomena (CEIDP), 19-22 Oct. 2014 2014. 715-718.

KOHL, J. G. & SINGER, I. L. 1999. Pull-off behavior of epoxy bonded to silicone duplex coatings. *Progress in organic coatings,* 36**,** 15-20.

LEMKE, E. 2012. A critical review of partial-discharge models. *IEEE Electrical Insulation Magazine,* 28**,** 11-16.

LÉONARD, F., STEIN, J., WILKINSON, A. & WITHERS, P. 2012. 3D characterisation of void distribution in resin film infused composites. *Conferene on Industrial Computed Tomography*.

LEROY, C. & RANCOITA, P.-G. 2011. *Principles of radiation interaction in matter and detection*, World Scientific.

LEWIS, T. J. 1994. Nanometric dielectrics. *IEEE Transactions on Dielectrics and Electrical Insulation,* 1**,** 812-825.

LI, Z., OKAMOTO, K., OHKI, Y. & TANAKA, T. 2010. Effects of nano-filler addition on partial discharge resistance and dielectric breakdown strength of Micro-Al2O3Epoxy composite. *IEEE Transactions on Dielectrics and Electrical Insulation,* 17**,** 653-661.

MALIK, N. H., AL-ARAINY, A. A., QURESHI, M. I. & PAZHERI, F. R. Calculation of electric field distribution at high voltage cable terminations. 2010 International Conference on High Voltage Engineering and Application, 11-14 Oct. 2010 2010. 24-27.

MARKOWICZ, A. A. 2001. X-ray physics. *Handbook of X-Ray Spectrometry, Second Edition.* CRC Press.

MARTIN, D., WANG, Z. D., DYER, P., DARWIN, A. W. & JAMES, I. R. A Comparative Study of the Dielectric Strength of Ester Impregnated Cellulose for Use in Large Power Transformers. 2007 IEEE International Conference on Solid Dielectrics, 8-13 July 2007 2007. 294-297.

MOHANTY, A. & SRIVASTAVA, V. K. 2013. Dielectric breakdown performance of alumina/epoxy resin nanocomposites under high voltage application. *Materials & Design,* 47**,** 711-716.

MONZEL, W. J., HOFF, B. W., MAESTAS, S. S., FRENCH, D. M. & HAYDEN, S. C. 2015. Dielectric breakdown of additively manufactured polymeric materials. *IEEE Transactions on Dielectrics and Electrical Insulation,* 22**,** 3543-3549.

NAIDU, M. S. 2013. *High voltage engineering*, Tata McGraw-Hill Education.

NELSON, J. K., HU, Y. & THITICHAROENPONG, J. Electrical properties of TiO/sub 2/ nanocomposites. 2003 Annual Report Conference on Electrical Insulation and Dielectric Phenomena, 19-22 Oct. 2003 2003. 719-722.

NIEMEYER, L. 1995. A generalized approach to partial discharge modeling. *IEEE Transactions on Dielectrics and Electrical Insulation,* 2**,** 510-528.

OKABE, S., UETA, G., UTSUMI, T. & NUKAGA, J. 2015. Insulation characteristics of GIS insulators under lightning impulse with DC voltage superimposed. *IEEE Transactions on Dielectrics and Electrical Insulation,* 22**,** 1-9.

OKUBO, H. & HAYAKAWA, N. 2005. A novel technique for partial discharge and breakdown investigation based on current pulse waveform analysis. *IEEE Transactions on Dielectrics and Electrical Insulation,* 12**,** 736-744.

OKUZUMI, S., MURAKAMI, Y., NAGAO, M., SEKIGUCHI, Y., REDDY, C. C. & MURATA, Y. DC Breakdown Strength and Conduction Current of MgO/LDPE Composite Influenced by Filler Size. 2008 Annual Report Conference on Electrical Insulation and Dielectric Phenomena, 26-29 Oct. 2008 2008. 722-725.

OMRANI, A., SIMON, L. C. & ROSTAMI, A. A. 2009. The effects of alumina nanoparticle on the properties of an epoxy resin system. *Materials Chemistry and Physics,* 114**,** 145-150.

OSMOKROVIC, P., VASIC, A. & ZIVIC, T. 2005. The influence of the electric field shape on the gas breakdown under low pressure and small inter-electrode gap conditions. *IEEE Transactions on Plasma Science,* 33**,** 1677-1681.

PAN, C., CHEN, G., TANG, J. & WU, K. 2019. Numerical modeling of partial discharges in a solid dielectric-bounded cavity: A review. *IEEE Transactions on Dielectrics and Electrical Insulation,* 26**,** 981-1000.

PARAMANE, A. S. & KUMAR, K. S. 2016. A review on nanocomposite based electrical insulations. *Transactions on electrical and electronic materials,* 17**,** 239-251.

PARK, J.-J., SHIN, S.-S., YOON, C.-Y., LEE, J.-Y. & PARK, J.-E. 2015. Electrical and mechanical properties of epoxy/micro-sized alumina composite and the effect of nano-sized alumina on those properties. *Transactions on Electrical and Electronic Materials,* 16**,** 260-263.

PREETHA, P. & THOMAS, M. J. 2011. AC breakdown characteristics of epoxy nanocomposites. *IEEE Transactions on Dielectrics and Electrical Insulation,* 18**,** 1526-1534.

RAICEVIC, N. B. Electrical field and potential distribution at the cable termination. PowerTech Budapest 99. Abstract Records. (Cat. No.99EX376), 29 Aug.-2 Sept. 1999 1999. 215.

RAMU, T. S. & NAGAMANI, H. N. 2014. Alumina and silica based epoxy nano-composites for electrical insulation. *IEEE Transactions on Dielectrics and Electrical Insulation,* 21**,** 236-243.
ROJEK, J., BREITE, C., SWOLFS, Y. & LAIARINANDRASANA, L. 2020. Void growth measurement and modelling in a thermosetting epoxy resin using SEM and tomography techniques. *Continuum Mechanics and Thermodynamics,* 32**,** 471-488.
SARATHI, R., SAHU, R. & RAJESHKUMAR, P. 2007. Understanding the thermal, mechanical and electrical properties of epoxy nanocomposites. *Materials Science and Engineering: A,* 445**,** 567-578.
SCOTT, A., SINCLAIR, I., SPEARING, S. M., MAVROGORDATO, M. N. & HEPPLES, W. 2014. Influence of voids on damage mechanisms in carbon/epoxy composites determined via high resolution computed tomography. *Composites Science and Technology,* 90**,** 147-153.
SEONG, J. K., SEO, I. J., HWANG, J. S. & LEE, B. W. 2012. Comparative Evaluation Between DC and AC Breakdown Characteristic of Dielectric Insulating Materials in Liquid Nitrogen. *IEEE Transactions on Applied Superconductivity,* 22**,** 7701504-7701504.
SHIBUYA, Y., ZOLEDZIOWSKI, S. & CALDERWOOD, J. H. 1977. Void formation and electrical breakdown in epoxy resin. *IEEE Transactions on Power Apparatus and Systems,* 96**,** 198-207.
SINGHA, S. & THOMAS, M. J. 2008. Dielectric properties of epoxy nanocomposites. *IEEE Transactions on Dielectrics and Electrical Insulation,* 15**,** 12-23.
SISODIA, S. M., GARCEA, S., GEORGE, A., FULLWOOD, D., SPEARING, S. & GAMSTEDT, E. 2016. High-resolution computed tomography in resin infused woven carbon fibre composites with voids. *Composites Science and Technology,* 131**,** 12-21.
TANG, J.-M., LEE, W. I. & SPRINGER, G. S. 1987. Effects of cure pressure on resin flow, voids, and mechanical properties. *Journal of composite materials,* 21**,** 421-440.
WANG, F., ZHANG, T., LI, J., ZEESHAN, K. M., HE, L., HUANG, Z. & HE, Y. 2019a. DC breakdown and flashover characteristics of direct fluorinated epoxy/Al2O3 nanocomposites. *IEEE Transactions on Dielectrics and Electrical Insulation,* 26**,** 702-737.
WANG, S., LI, A., XING, Y., LI, K. & LI, Z. 2019b. Surface Potential and Breakdown Characteristics of Epoxy/AlN Nanocomposites Under DC and Pulse Voltages. *IEEE Transactions on Applied Superconductivity,* 29**,** 1-5.
WEARNE, L. S., RAPAGNA, S., TAYLOR, M. & PERILLI, E. 2022. Micro-CT scan optimisation for mechanical loading of tibia with titanium tibial tray: A digital volume correlation zero strain error analysis. *Journal of the Mechanical Behavior of Biomedical Materials,* 134**,** 105336.
WETHERILL, Y. B., AKINGBEMI, B. T., KANNO, J., MCLACHLAN, J. A., NADAL, A., SONNENSCHEIN, C., WATSON, C. S., ZOELLER, R. T. & BELCHER, S. M. 2007. In vitro molecular mechanisms of bisphenol A action. *Reproductive toxicology,* 24**,** 178-198.
WOOI, C. L., ABDUL-MALEK, Z., AHMAD, N. A. & MOKHTARI, M. Characteristic of preliminary breakdown preceding negative return stroke in Malaysia. 2015 IEEE Conference on Energy Conversion (CENCON), 19-20 Oct. 2015 2015. 112-115.
WU, J., JIN, H., MOR, A. R. & SMIT, J. The effect of frequency on the dielectric breakdown of insulation materials in HV cable systems. 2017 International Symposium on Electrical Insulating Materials (ISEIM), 2017. IEEE, 251-254.
YIN, Y., DONG, X., LI, Z. & LI, X. The Effect of Electrically Prestressing on DC Breakdown Strength in the Nanocomposite of Low-density Polyethylene / nano-SiOx. 2007 IEEE International Conference on Solid Dielectrics, 8-13 July 2007 2007. 372-376.
ZARRELLI, M., SKORDOS, A. A. & PARTRIDGE, I. K. 2002. Investigation of cure induced shrinkage in unreinforced epoxy resin. *Plastics, rubber and composites,* 31**,** 377-384.

Appendix:

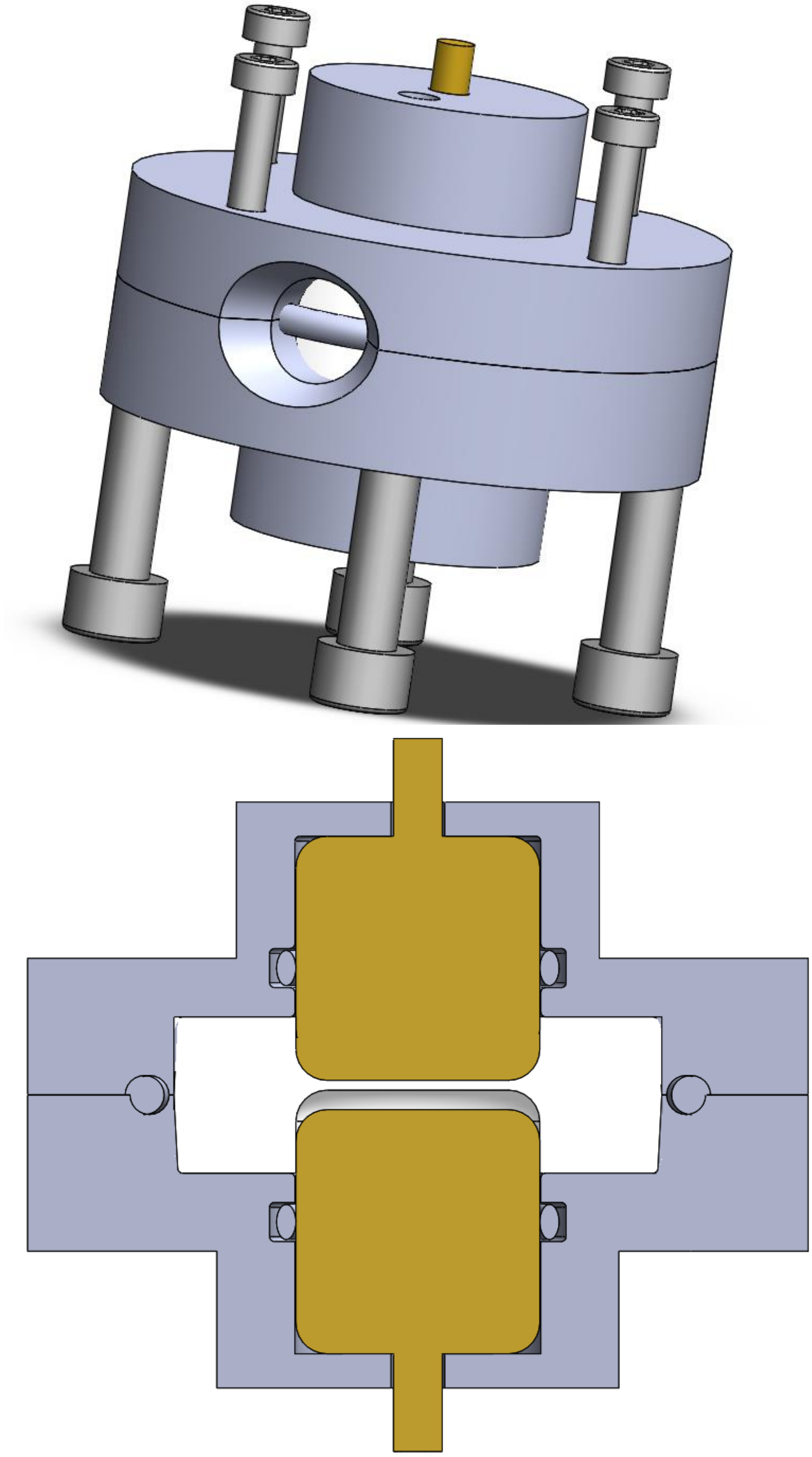

Figure 22 – Solidworks render of an electrode mould (upper) and a cross section of the mould (lower). The thinner fasteners hold the mould halves together, the thicker fasteners are used to assist in opening the mould.

Figure 23 - Bubbles present in a sample of 2% nanocomposite (left) and 0.5% (right). Bubbles were present throughout the experiment, for all samples bar the Megapoxy E slow samples which were mixed and potted under vacuum.

Figure 24 – A dissection of neat epoxy sample #3, which survived 593 cycles of ALT pulses before arcing, causing the black charring between electrodes (left). On the right, neat epoxy sample #4, which survived 609 pulses before failure, showing physical damage to the epoxy caused by dielectric breakdown (indicated by the red arrow).

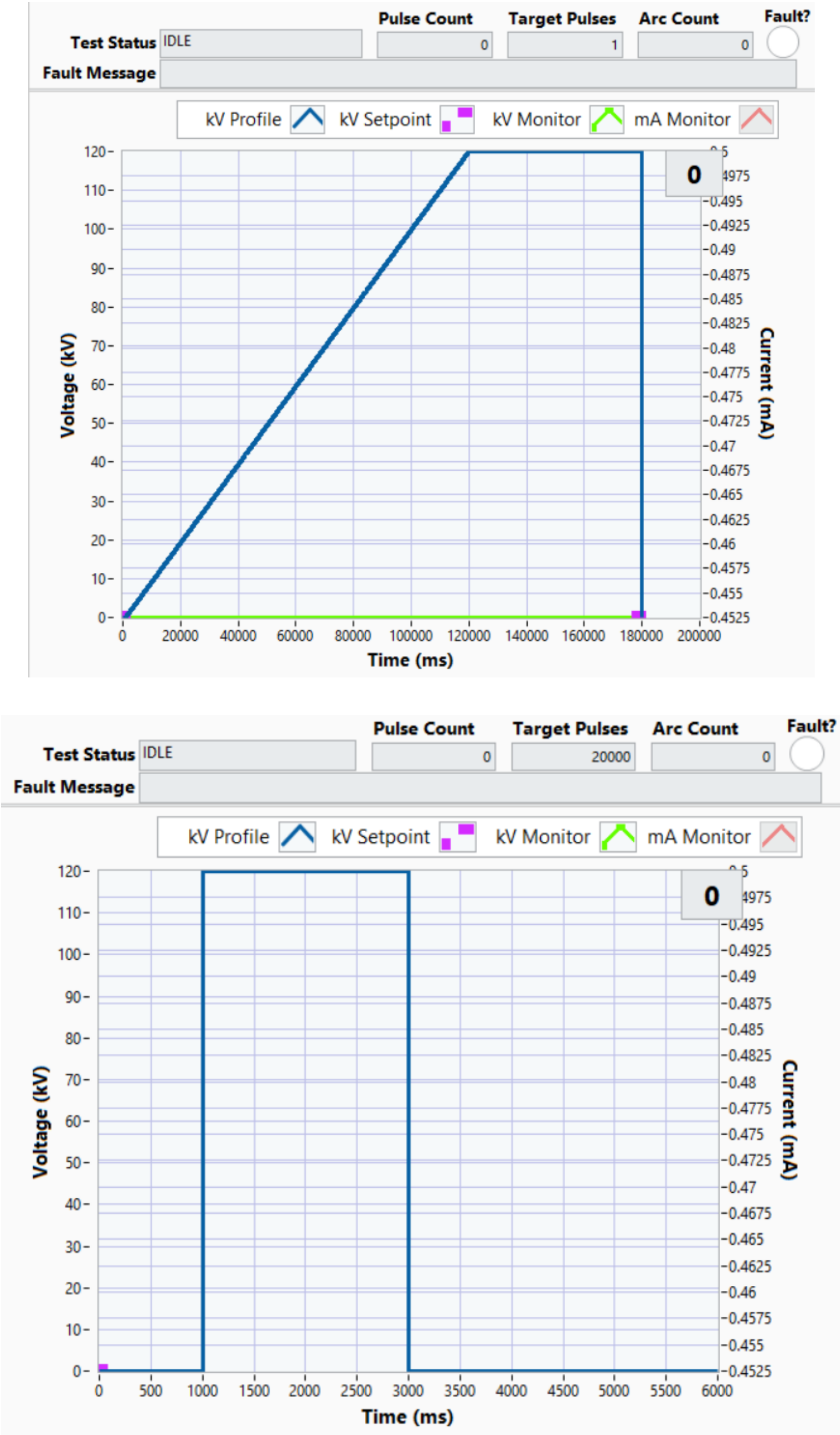

Figure 25 – Spellman GUI screenshot of the withstand test parameters (upper, ramp pulse and hold at 120kV), and the ALT test parameters (lower, repeated step pulses at 120kV).

Arduino code used to measure temperature data:

```
// Quick and dirty code to TX temperature info over serial every
30s.


#include <math.h>


void setup () {
  Serial.begin (9600);
}


void loop () {
  // I have connected thermistor output to Analog pin 0 on Arduino.
  Serial.println (Thermister (analogRead (0)));
  delay (30000);
}


// Grab ADC value, convert to usable value:
double Thermister (int RawADC) {
  double Temp;
  // Copied directly from manufacturer's website, these weird
numbers give quite accurate results!
  Temp = log (((10240000/RawADC) - 10000));
  Temp = 1 / (0.001129148 + (0.000234125 + (0.0000000876741 * Temp *
Temp)) * Temp);
  // Convert Kelvin to Celsius
  Temp = Temp - 273.15;
  return Temp;
}


// EOF
```

Python code used to receive the Arduino temperature data and log it:

```
# Code to acquire temp data from Arduino over serial in log into a
text file

import serial

from datetime import datetime

serialPort = serial.Serial(port = "COM14", baudrate=9600,
      bytesize=8, timeout=2, stopbits=serial.STOPBITS_ONE)


# Sit here and gather data

while(1):

    # Wait until there is data waiting in the serial buffer

    if(serialPort.in_waiting > 0):


        # Read data out of the buffer until a carraige return / new
line is found (Arduino adds these at end of TX).

        serialString = serialPort.readline()


        # Kill newline spam for excel compatibility.

        serialString = serialString.decode('Ascii')

        serialString = serialString.strip("\n")


        # Print the contents of the serial data (sanity checking).

        print(serialString)


        # Append the data into text file, literally named test.

        textfile = open("test.txt", "a")

        now = datetime.now()

        textfile.write(now.strftime("%H:%M:%S "))

        textfile.write(serialString)

        textfile.close()


# EOF
```

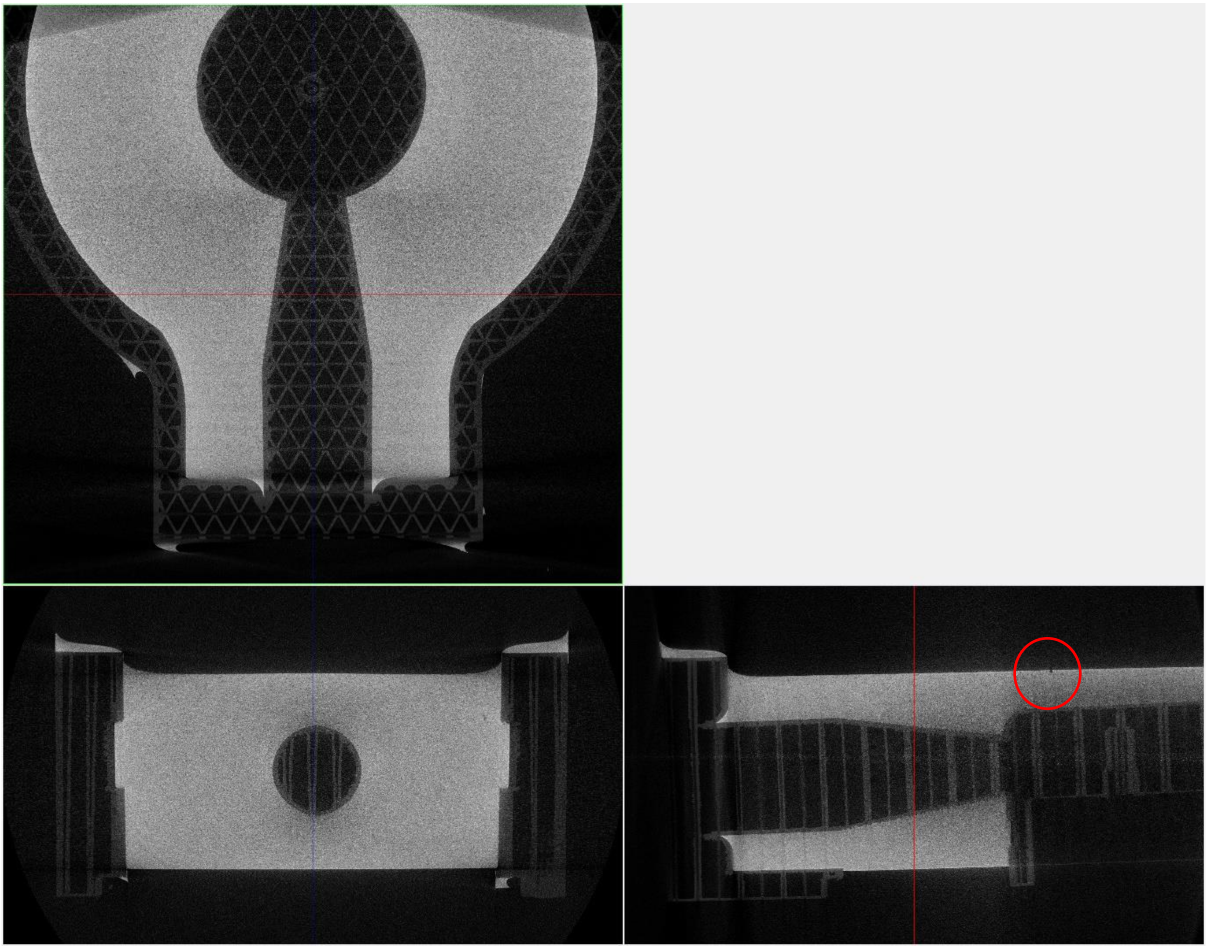

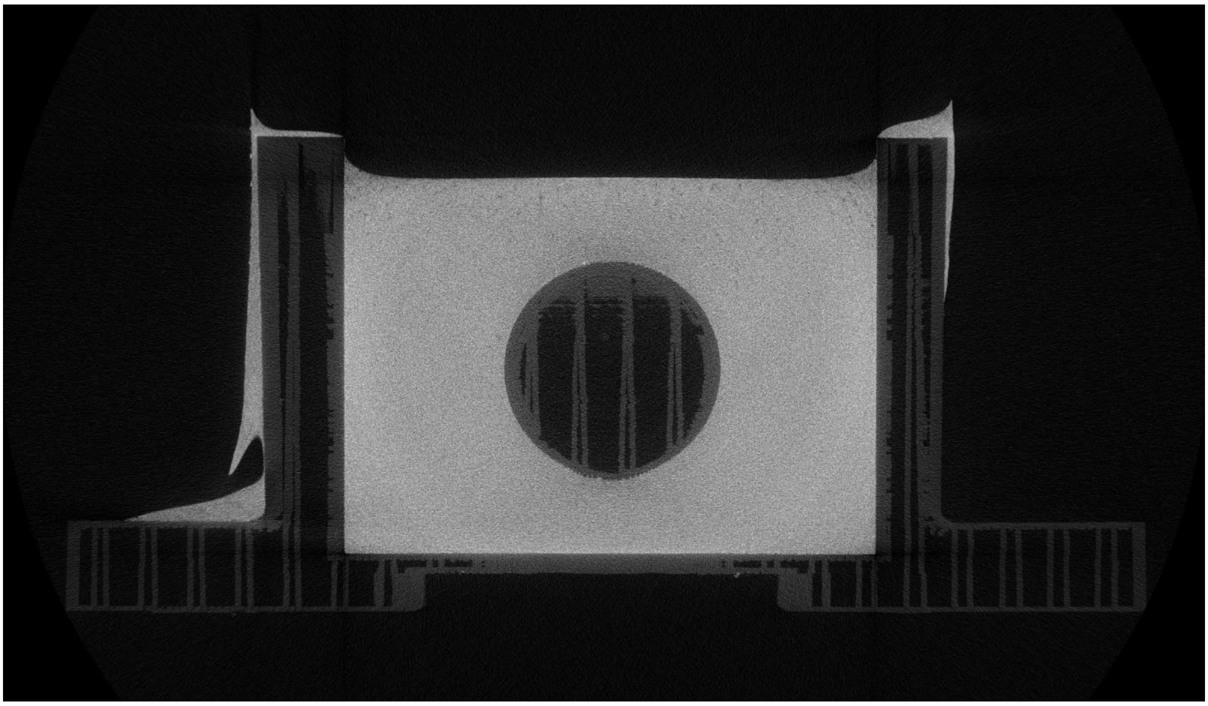

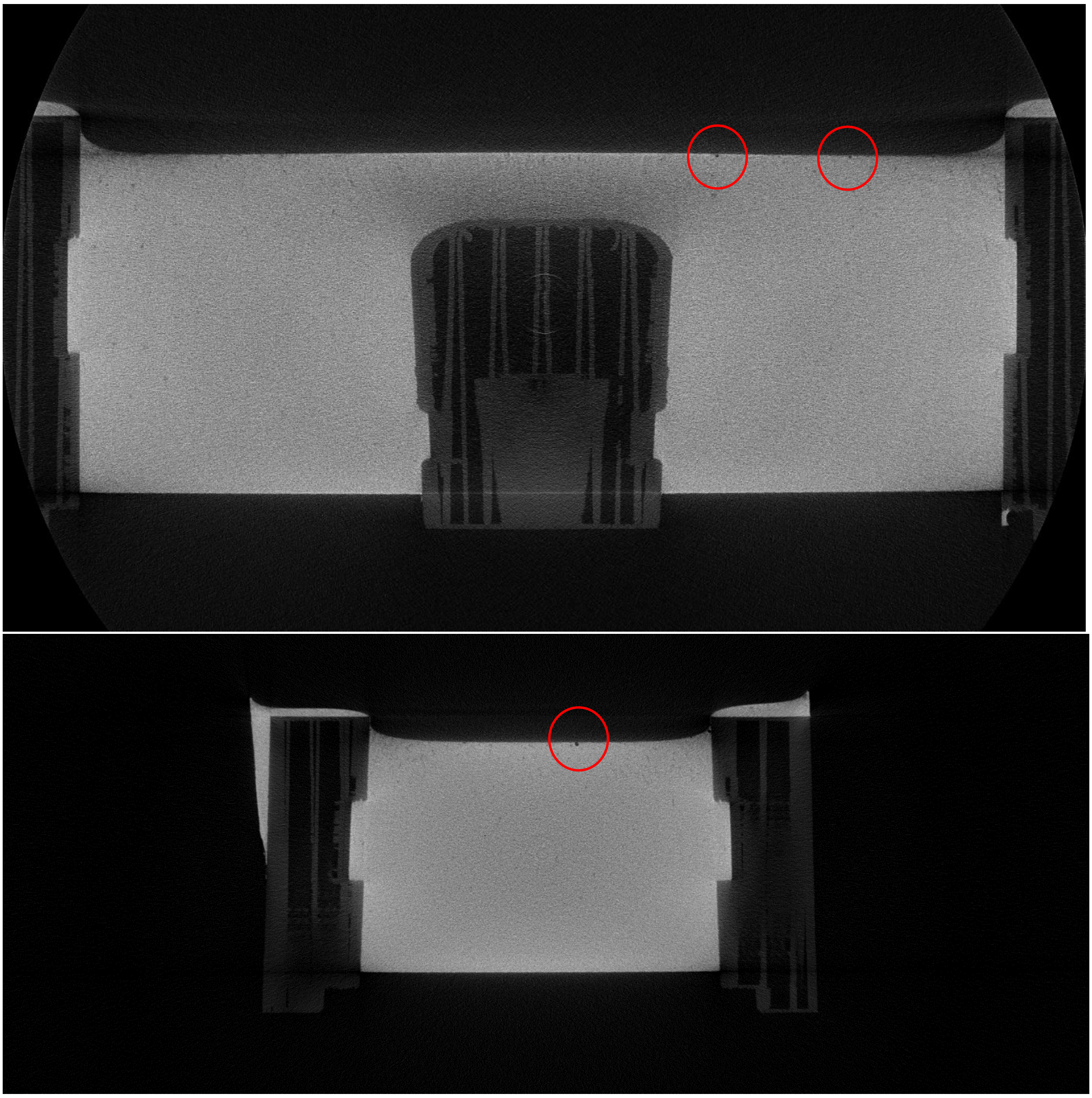

Figure 26 – Reconstructed Micro-CT image slices of the 3D printed proxy connector. Note the general consistency of the bulk of the epoxy (lighter regions), however a few bubbles can be seen at the top of the connector and have been circled in red. X-ray Micro-CT settings (Nikon XT H 225 ST, based in Flinders University Tonsley campus): 24µm resolution, 4s exposure, 215kV source voltage, 112 µA source current, 0.25mm tin filter. 2000 projections per full rotation over 360 degrees. Detector size was 4056 x 4056 pixels.

Figure 27 - Solidwork renders of the cable connector:

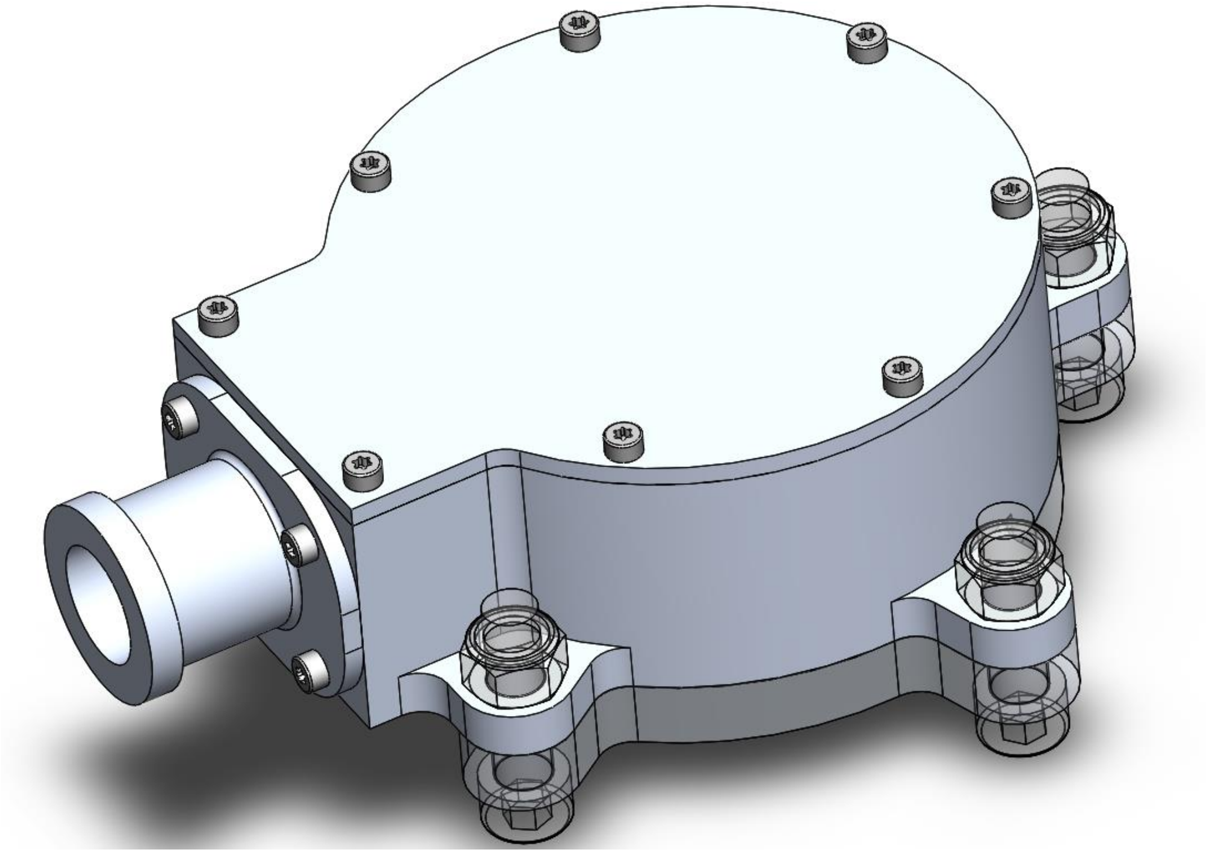

Above – The entire connector with fasteners and shut-off plate (transparent), rear view.

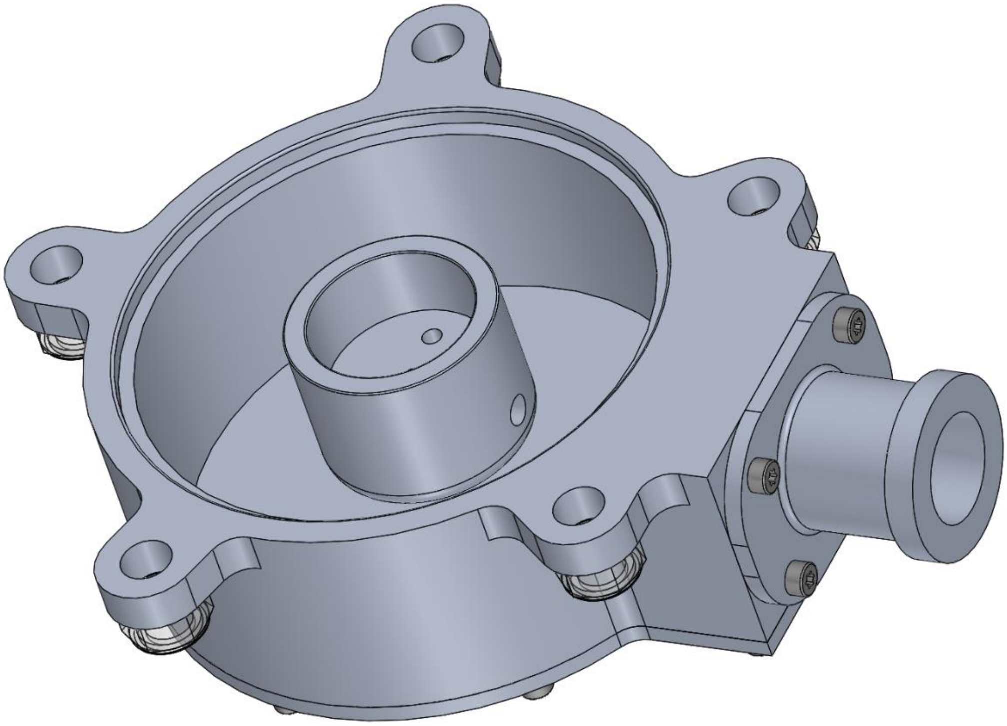

Above – Front view of the connector. Epoxy and high-voltage cable not modelled.

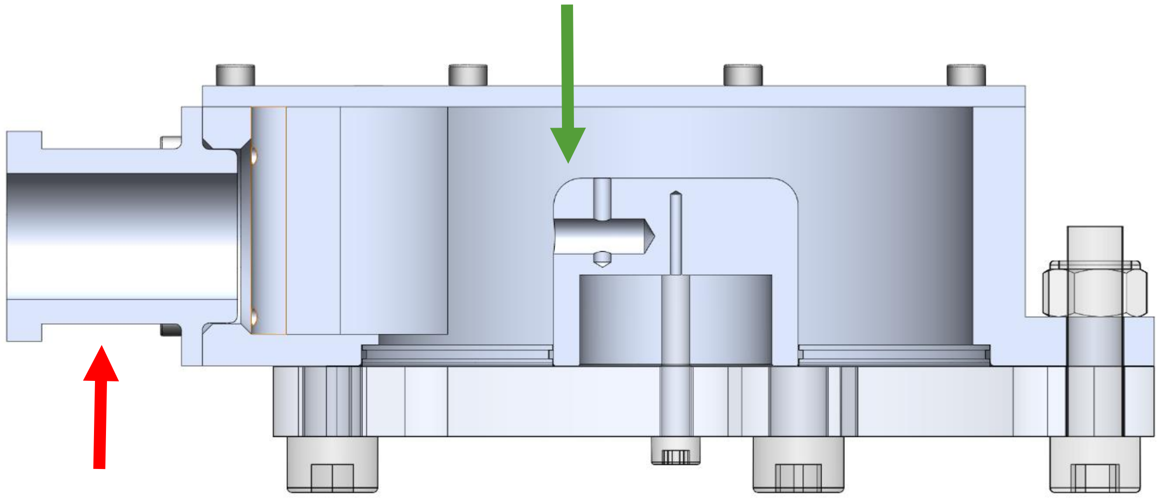

Above - Cross-section view of the cable connector. The high-voltage cable passes through the earthing interface tube (red arrow), and the conductors of which insert into the left hole on the centre pin (green arrow), held in place with a small grubscrew from above. The transparent shut-off plate is shown, note the grooves on the raised surface to allow O-ring fitting. A fastener can be seen holding the centre pin flush to the shut-off plate.

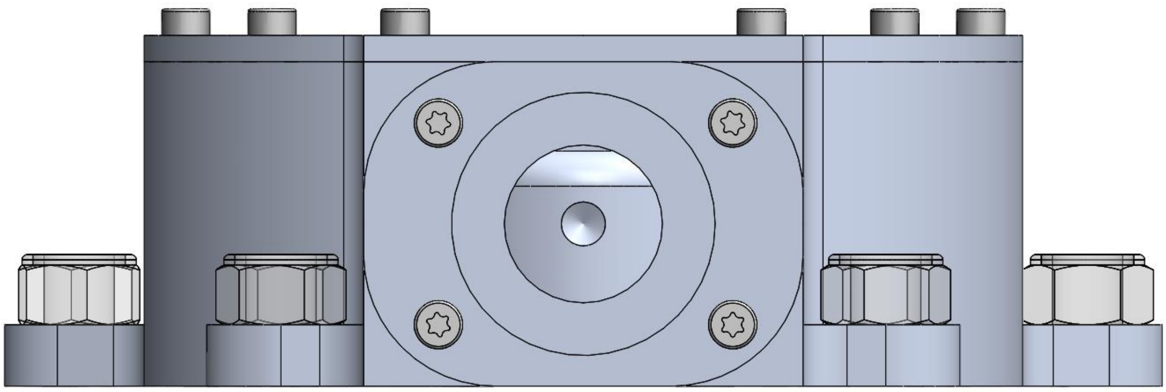

Above – view through the earthing interface, the hole on the centre pin where the high-voltage cable inserts can be clearly seen.

Figure 28 – Above images: Touching up the damage caused by the machining process by adding small amounts of new epoxy prior to sanding by hand (left), and after sanding (right). Below images: Applying a silicon gasket and silicon grease to the blanking plate (left), and interfacing the newly potted anode cable connector to the plate for testing (right).